Supporting Information

Facile preparation of high-efficiency peroxidase mimics: modulation of the catalytic microenvironment of LDH nanozymes through defect engineering induced by amino acid intercalation

Dong Han,[†a] Kui Yang,[†b] Lanlan Chen,[a] Zhaosheng Zhang,[b] Chen Wang,[a] Hongyuan Yan,*[b] and Jia Wen*[a]

State Key Laboratory of New Pharmaceutical Preparations and Excipients, Key Laboratory of Medicinal Chemistry and Molecular Diagnosis of the Ministry of Education, College of Pharmaceutical Science, Hebei University, Baoding 071002, P. R. China, E-mail: wenjiahbu@163.com.

State Key Laboratory of New Pharmaceutical Preparations and Excipients, Key Laboratory of Medicinal Chemistry and Molecular Diagnosis of Ministry of Education, College of Chemistry and Materials Science, Hebei University, Baoding 071002, P. R. China, E-mail: yanhy@hbu.edu.cn.

† These authors contribute equally to this work.

1. Materials and Instruments

$CoCl_2 \cdot 6H_2O$, $FeCl_2 \cdot 4H_2O$, NaOH and H_2O_2 (30 wt%) were obtained from Damao Chemical Reagent Co., Ltd (Tianjin, China). Acetic acid (HAc) and sodium acetate (NaAc) were purchased from Fuchen Chemical Reagent Co., Ltd (Tianjin, China). *p*-benzoquinone (*p*-BQ), terephthalic acid (TA), L-Alanine (L-Ala, **A**), L-Arginine (L-Arg, **R**), L-Asparagine (L-Asn, **N**), L-Aspartic acid (L-Asp, **D**), L-Glutamic acid (L-Glu, **E**), L-Glycine (L-Gly, **G**), L-Histidine (L-His, **H**), L-Isoleucine (L-Ile, **I**), L-Leucine (L-Leu, **L**), L-Serine (L-Ser, **S**), L-Threonine (L-Thr, **T**), L-Valine (L-Val, **V**), D-Cysteine (D-Cys), Cystine (Cys-Cys, **C**-**C**), N-Acetyl-L-Cysteine (Acet-L-Cys) were purchased form Bide Pharmatech Co., Ltd (Shanghai, China). 3,3',5,5'-Tetramethylbenzidine (TMB), L-Cysteine (L-Cys, **C**), L-Glutamine (L-Gln, **Q**), L-Lysine (L-Lys, **K**), L-Methionine (L-Met, **M**), L-Phenylalanine (L-Phe, **F**), L-Proline (L-Pro, **P**), L-Tryptophan (L-Trp, **W**), Tyrosine (L-Tyr, **Y**) and ascorbic acid (AA) were obtained from Annaiji Chemical Co., Ltd (Shanghai, China). Deionized (DI) water (18.2 MΩ·cm) was used throughout the experiments. 0.2 mol L^{-1} HAc-NaAc buffer solutions with different pH values were prepared in advance for use.

The morphology of nanozymes were examined by a transmission electron microscopy (TEM, TALOS F200, Thermo Fisher, USA). High-resolution TEM (HRTEM) images and elemental mapping images were obtained on a TALOS F200 high-resolution TEM system operating at 200 kV (Thermo Fisher, USA). The thickness of the nanozymes were measured on a Bruker Dimension Icon atomic force microscope (AFM, Bruker, Germany). X-ray diffraction (XRD) patterns were measures by D8 ADVANCE instrument (Bruker, Germany) at 40 kV and 40 mA with Cu K radiation (λ = 0.15406 nm, 5°/min) in the 2θ range of 3-70°. Fourier-transform infrared spectrometer (FT-IR, Nicolet iS10, Thermo Fisher, USA) spectra were recorded in the wavenumber range of 4000 to 400 cm^{-1} using KBr. The elemental compositions were analyzed by inductively coupled plasma optical emission spectrometry (ICP-OES, Agilent 5110, Agilent, USA). Surface composition and chemical states of the nanozymes were performed by X-ray photoelectron spectroscopy (XPS, Thermo ESCALAB 250XI, Thermo Fisher, USA) and all of the binding energy data were calibrated by C 1s (284.8 eV). Electron paramagnetic resonance (EPR) spectra were obtained from Bruker A300 (Bruker, Germany). UV-vis absorbance spectra were tested by a UH5300 spectrophotometer (Hitachi, Japan). The surface zeta potential of the as-prepared nanozymes was investigated using ZETAsizer Nanolink (SZ900, Malvern Instruments

Limited, U.K.). X-ray absorption spectroscopy (XAS) measurements were carried out at the XAS Beamline of the Australian Synchrotron in Melbourne using a set of liquid nitrogen cooled Si (111) monochromator crystals. The electron beam energy was 3.0 GeV. With the associated beamline optics (Si-coated collimating mirror and Rh-coated focusing mirror), the harmonic content of the incident X-ray beam was negligible. Data was collected using transmission mode, and the energy was calibrated using a Co foil. The beam size was about 1x1mm. A single XAS scan took about 1 h. Scanning electron microscopy (SEM) measurements were conducted on the Nova NanoSEM450 (FEI, Germany).

2. Methods

2.1 Preparation of CoFe-LDH nanozyme

Firstly, $CoCl_2$•$6H_2O$ (2 mmol) and $FeCl_2$•$4H_2O$ (1 mmol) were dissolved in 30 mL of DI water and the solution was named as solution A. Secondly, NaOH (4 mmol) was dissolved in 20 mL of DI water to obtain solution B. Afterwards, solution A was slowly added to solution B to make the pH value of the solution to be 8.0-9.0. Meanwhile, nitrogen (N_2) was injected into the drip process. The final solution was stirred for 30 min and then continued to stirred for 6 h at 80℃. Finally, the precipitation was collected by centrifugation and washed with DI water to pH<8. The product obtained after freeze-drying was CoFe-LDH nanozyme[1].

2.2 Preparation of L-AA-LDH nanozymes

Firstly, $CoCl_2$•$6H_2O$ (2 mmol) and $FeCl_2$•$4H_2O$ (1 mmol) were dissolved in 30 mL of DI water and the solution was named as solution A. Secondly, various amino acids (AA, 1 mmol) and NaOH (4 mmol) was dissolved in 20 mL of DI water to obtain solution B. Afterwards, solution A was slowly added to solution B to make the pH value of the solution to be 8.0-10.0. Meanwhile, nitrogen (N_2) was injected into the drip process. The final solution was stirred for 30 min and then continued to stirred for 6 h at 80℃. Finally, the precipitation was collected by centrifugation and washed with DI water to pH<8. The product obtained after freeze-drying was named as L-AA-LDH nanozyme[2].

2.3 Preparation of **C**-LDH nanozymes

Firstly, $CoCl_2$•$6H_2O$ (2 mmol) and $FeCl_2$•$4H_2O$ (1 mmol) were dissolved in 30 mL of DI water and the solution was named as solution A. Secondly, various L-Cys derivates (**C**, 1 mmol) and NaOH (4 mmol) was dissolved in 20 mL of DI water to obtain solution B. Afterwards, solution A

was slowly added to solution B to make the pH value of the solution to be 8.0-10.0. Meanwhile, nitrogen (N_2) was injected into the drip process. The final solution was stirred for 30 min and then continued to stirred for 6 h at 80℃. Finally, the precipitation was collected by centrifugation and washed with DI water to pH<8. The product obtained after freeze-drying was named as **C**-LDH nanozyme.

2.4 POD-like activity of CoFe-LDH nanozyme and L-AA-LDH nanozymes

The peroxidase (POD)-like activity of CoFe-LDH nanozyme and different L-AA-LDH nanozymes were carried out through the oxidation reaction of TMB in the presence of H_2O_2. Typically, 120 μL of TMB ethanol solution (5 mM), 120 μL of H_2O_2 (5 mM) and 30 μL of nanozymes suspension (1.00 mg mL^{-1}) were added into 2730 μL of acetate buffer solution (HAc-NaAc, 0.2 M, pH = 3.0), respectively. The mixture was incubated at room temperature for 10 min and the absorbance intensities at 652 nm of their UV-Visible spectroscopy were monitored.

2.5 Oxidase-like activity of CoFe-LDH nanozyme and L-AA-LDH nanozymes

The oxidase-like property of CoFe-LDH nanozyme and different L-AA-LDH nanozymes were carried out through the oxidation reaction of TMB. Typically, 120 μL of TMB ethanol solution (5 mM) and 30 μL of nanozymes suspension (1.00 mg mL^{-1}) were added into 2850 μL of HAc-NaAc buffer (0.2 M, pH = 3.0), respectively. The mixture was incubated at room temperature for 10 min and the absorbance intensities at 652 nm of their UV-Visible spectroscopy were monitored.

2.6 Optimization of test conditions

In order to achieve the optimal catalytic activity of nanozymes, pH values of HAc-NaAc buffer solution and incubation temperature were optimized. 30 μL of **C**-LDH aqueous solution (1 mg mL^{-1}), 120 μL of TMB (5 mM) and 120 μL of H_2O_2 (5 mM) were added into 0.2 M HAc-NaAc buffer with different pH values (2.0, 2.5, 3.0, 3.5, 4.0, 4.5, 5.0 and 5.5) and incubated at room temperature for 10 min. It was then transferred to a cuvette for UV-vis spectroscopy test. 30 μL of **C**-LDH nanozyme aqueous solution (0.25 mg mL^{-1}), 120 μL of TMB (5 mM) and 120 μL of H_2O_2 (5 mM) were added in turn into 0.2 M HAc-NaAc buffer (pH 3.0) and incubated for 10 min at different temperatures (25, 30, 35, 40, 45, 50, 55, 60 and 65℃). It was then transferred to a cuvette for UV-vis spectroscopy test.

2.7 Stability and reproducibility tests of LDH nanozymes

In order to study the stability of LDH nanozymes, the solutions and solids of CoFe-LDH

nanozyme，L-**C**-LDH nanozyme and Me-L-**C**-LDH nanozyme were stored at 4℃, the activity of which were tested at intervals through recording the absorbance of the reaction solution at 652 nm and compared. The catalytic activity of the LDH nanozymes on the first day was set at 100%[3].

In order to evaluate the reproducibility of LDH nanozymes, an appropriate amount of LDH nanozymes was weighed and added to 5 mL of HAc-NaAc buffer (0.2 M, pH = 3.0). Then TMB (5 mM) and H_2O_2 (5 mM) were added into the mixture solution to make the final concentration of LDH nanozymes in the reaction system was 1 mg mL^{-1}, the final concentration of TMB and H_2O_2 was 0.2 mM. Then the solution was reacted at 25℃ for 5 min per cycle. After centrifugation at 12000 rpm for 3 min, the supernatant and precipitation were collected respectively. The absorbance of the supernatant at 652 nm was measured after the supernatant was diluted twice. The collected precipitate was washed with DI water by centrifugation (12000 rpm, 5 min). The product was freeze-dried, re-quantified and used in the next reaction cycle. The test was carried out in 5 cycles with 3 parallel groups in each cycle.

2.8 Michaelis-Menten kinetics test

In order to detect the affinity of different LDH nanozymes to substrate TMB and H_2O_2, the catalytic kinetics of LDH nanozymes were studied at room temperature and 37℃, respectively. The catalytic rates of various L-AA-LDH nanozymes at different concentrations of TMB and H_2O_2 were measured, and Michaelis constant (K_m) and maximum reaction rate (V_{max}) were calculated.

Under the optimal conditions with various concentrations of TMB (0.2 mM-2.0 mM) and fixed concentration of H_2O_2 (1.50 mM) or with various concentrations of H_2O_2 (0.2 mM-2.0 mM) and fixed concentration of TMB (1.50 mM), the kinetic tests were operated in time scan mode at 652 nm by microplate reader. The K_m and V_{max} were derived via the following equation:

$$\frac{1}{v} = \frac{K_m}{V_{max}[S]} + \frac{1}{V_{max}}$$

Where v was the initial velocity, V_{max} was the maximum velocity of reaction, K_m was the constant of Michaelis-Menten equation, and [S] was the concentration of the substrate.

2.9 Radicals scavenging experiments

To confirm the POD-like catalytic mechanism of LDH nanozymes, radicals scavenging experiments were performed. TH and *p*-BQ were used as scavengers for hydroxyl radicals (•OH)

and superoxide anion ($O_2^{\bullet-}$), respectively[4]. LDH nanozymes (10 μg mL^{-1}), TMB (0.2 mM), H_2O_2 (0.2 mM) and the selected scavenger at an appropriate concentration were used to detect the radical types related to the POD-like activity of LDH nanozymes.

The production of $^{\bullet}OH$ and $O_2^{\bullet-}$ intermediates during the POD-like reaction based on LDH nanozymes was monitored by EPR using DMPO as a spin trap. Typically, HAc-NaAc buffer (0.2 M, pH 3.0) containing 20 mM DMPO and 0.2 mM H_2O_2 was sealed in the presence or absence of LDH nanozymes (10 μg mL^{-1}). The EPR spectra were recorded after the above mixture reacted for 10 min at room temperature.

2.10 Density functional theory (DFT) calculations

The spin-polarized DFT[5, 6] calculations were performed using the Vienna Ab initio Simulation Package (VASP) based on the plane-wave basis sets with the projector augmented-wave (PAW) method[7, 8]. The exchange-correlation potential was treated by using a generalized gradient approximation (GGA) with the Perdew-Burke-Ernzerhof (PBE) parametrization[9]. The van der Waals correction of Grimme's DFT-D3 model was also adopted[10]. A vacuum region of about 12 Å was applied to avoid the interaction between adjacent images. The energy cutoff was set to be 450 eV. The Brillouin-zone integration was sampled with a single Gamma point (1 × 1 × 1). The structures were fully relaxed until the maximum force on each atom was less than 0.04 eV/Å, and the energy convergent standard was 10^{-6} eV. The Gibbs free energies of the intermediates in H_2O_2 evolution were calculated using the following expression:

$$\Delta G = \Delta E + \Delta E_{ZPE} + \Delta H_{0\rightarrow T} - T\Delta S$$

where ΔE denotes the change in electronic energy obtained from DFT, ΔE_{ZPE}, $\Delta H_{0\rightarrow T}$ and ΔS are the changes of the zero-point energy, the enthalpy and entropy at standard conditions (T= 298 K and at potential vs NHE).

2.11 Detection of H_2O_2 and AA based on LDH nanozymes

30 μg of LDH nanozymes (1 mg mL^{-1}), 120 μL of TMB (5 mM) and 120 μL of various concentrations of H_2O_2 (5-100 μM) were added in HAc-NaAc buffer (0.2 M, pH 3.0). After incubating at room temperature for 10 min, the absorbance of the reacted system at 652 nm was analyzed by UV-vis spectroscopy. The concentration of H_2O_2 was determined through a calibration curve of the absorbance.

The colorimetric detection of AA was similar to H_2O_2. 30 μg of LDH nanozymes (1 mg mL^{-}

^{1}), 120 μL of TMB (5 mM), 120 μL of H_2O_2 (5 mM) and 200 μL of various concentrations of AA (0.05-1 μM) were added in HAc-NaAc buffer (0.2 M, pH 3.0). After incubating at room temperature for 10 min, the absorbance of the reacted system at 652 nm was analyzed by UV-vis spectroscopy. The concentration of AA was determined through a calibration curve of the absorbance. The detection of limit (LOD) was calculated as 3σ/s, where s represents the slope of the linear curve and σ represents the blank signal standard deviation (SD).

To evaluate the selectivity of LDH nanozymes, 200 μL of CO_3^{2-}, SO_4^{2-}, SO_3^{2-}, Zn^{2+}, K^+, Gly, Val, Thr, Glu, Ala, Tyr, Leu (the final concentration of ions and amino acids were 500 μM and 100 μM, respectively) were pre-added in the detection system where the concentrations of AA was 60 μM.

2.12 *In vitro* antibacterial experiments

In all *in vitro* antibacterial experiments, the bacteria were culture in Luria-Bertani mediums. The absorbance at 600 nm was measured to determine the density of the bacterial population. The bacteria suspensions of *E. coli* and *S. aureus* at a concentration of 10^9 CFU mL^{-1} prepared in advance were randomly divided into eight groups: (1) bacteria; (2) bacteria + H_2O_2; (3) bacteria + CoFe-LDH; (4) bacteria + L-**C**-LDH; (5) bacteria + Me-L-**C**-LDH; (6) bacteria + CoFe-LDH + H_2O_2; (7) bacteria + L-**C**-LDH + H_2O_2; (8) bacteria + Me-L-**C**-LDH + H_2O_2. The final concentrations of LDH nanozymes were 250 μg mL^{-1} for *E. coli* and 200 μg mL^{-1} for *S. aureus*, respectively. The final concentrations of H_2O_2 were 1 mM for *E. coli* and 0.5 mM for *S. aureus*, respectively. Then the bacteria were incubated at 37°C under shaking with 150 rpm for 2 h in HAc-NaAc buffer (0.1 M, pH = 4.0). Subsequently, the bacteria suspensions were diluted, and 100 μL of dilutions were spread onto an agar culture plate for groups (1)-(8), respectively and incubated at 37°C for 14 h, and then the colonies were counted. Three replications of all experiments were conducted. The bacterial survival rate was calculated using the following equation: survival viability (%) = $N_t/N_c \times 100\%$, where N_t indicated the number of colonies formed in the experimental group and Nc represented the number of colonies formed in the control group[11].

The morphology of bacteria was observed by SEM. Firstly, the bacteria were incubated under different reactions at 37°C. After centrifugation (3500 rpm, 5 min), the bacterial were fixed in 2.5% glutaraldehyde solution overnight. Secondly, these bacteria were washed with phosphate buffered

solution (PBS, pH = 7.4) and then treated with different concentrations of alcohol solution (30%, 50%, 70%, 90%, 100%) for a period of 10 min each[11, 12]. Finally, the dehydrated bacterial suspensions were dropped on a silicon slice for morphology observation.

2.13 The quantification of amino acid

The reaction of α-amino acid with ninhydrin can form a large conjugated colored compound. At room temperature, the color reaction between amino acid and ninhydrin can be realized by adjusting the pH of the solution properly. First, the standard solution of L-Cys and Me-L-Cys (0.1-0.8 mg mL^{-1}), ninhydrin-ethanol chromogenic agent (1%) and NaOH (2 M) were prepared respectively. Then, 300 μL of ninhydrin-ethanol chromogenic agent was added into 3 mL of amino acid aqueous solution and shaked well. Finally, NaOH was slowly added until the solution became stable dark blue (pH>12). Measure the absorbance at 605 nm, and fit the linear curve of the content of amino acid and absorbance.

HCl (1 M) was added into the prepared solutions of L-**C**-LDH nanozyme and Me-L-**C**-LDH nanozyme (10 mg mL^{-1}), respectively and stirred at low speed for 6 h. And the supernatant was taken after centrifugation to detect the content of amino acid as above-mentioned.

3. Supplementary figures and tables

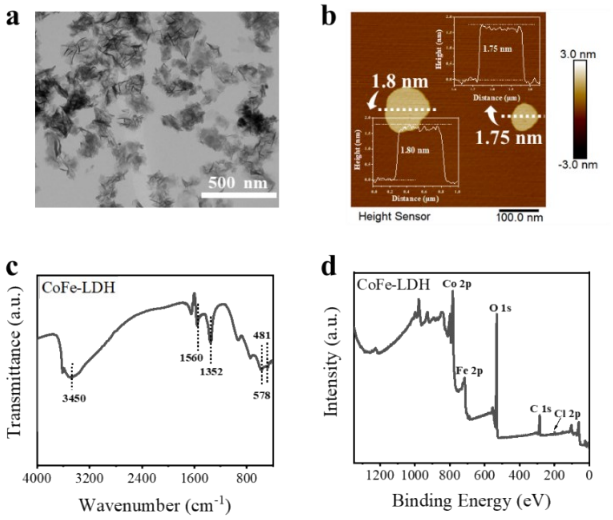

Figure S1. (a) TEM image, (b) AFM image, (c) FT-IR spectrum and (d) XPS survey spectrum of CoFe-LDH nanozyme.

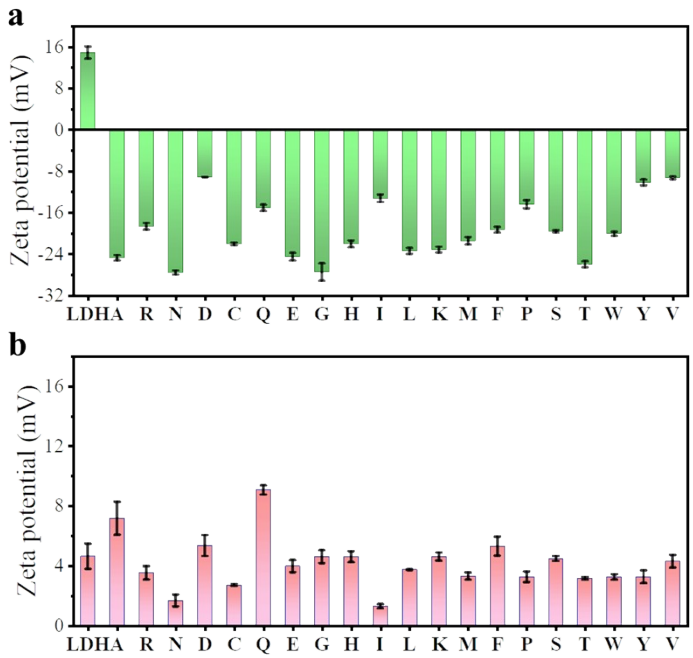

Figure S2. Zeta potentials of CoFe-LDH nanozyme and different L-AA-LDH nanozymes in (a) water and (b) acetate buffer (pH 3.0).

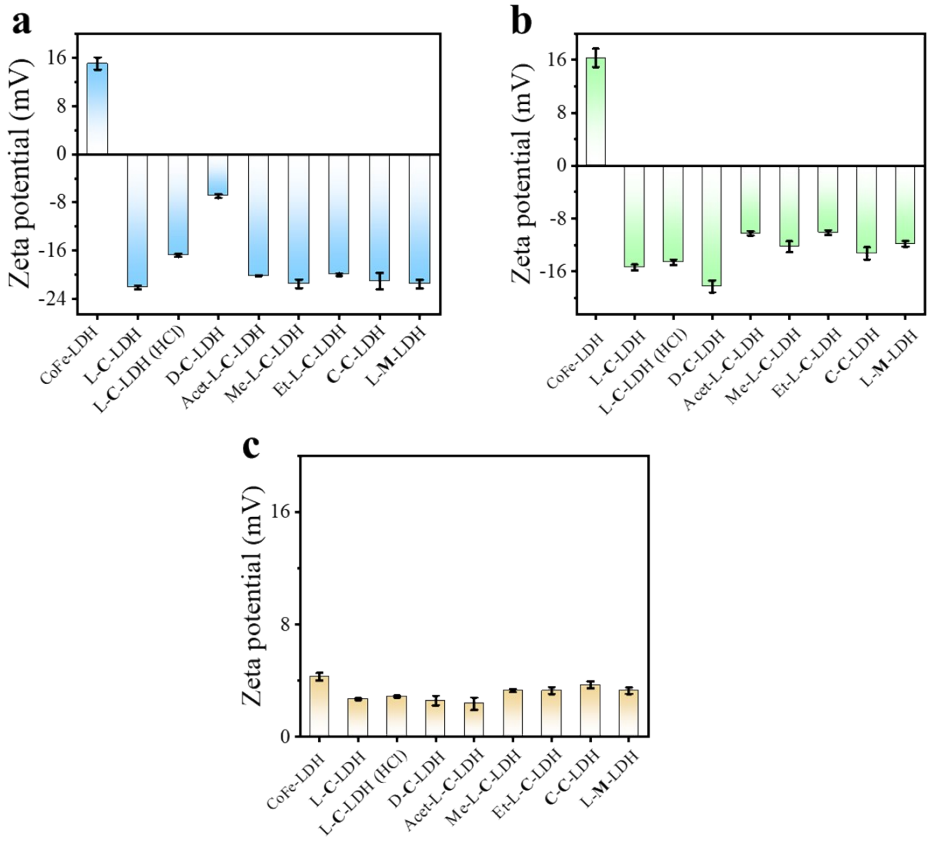

Figure S3. Zeta potentials of CoFe-LDH nanozyme and different **C**-LDH nanozymes in (a) water, (b) phosphate buffer (pH = 7.4) and (c) acetate buffer (pH = 3.0).

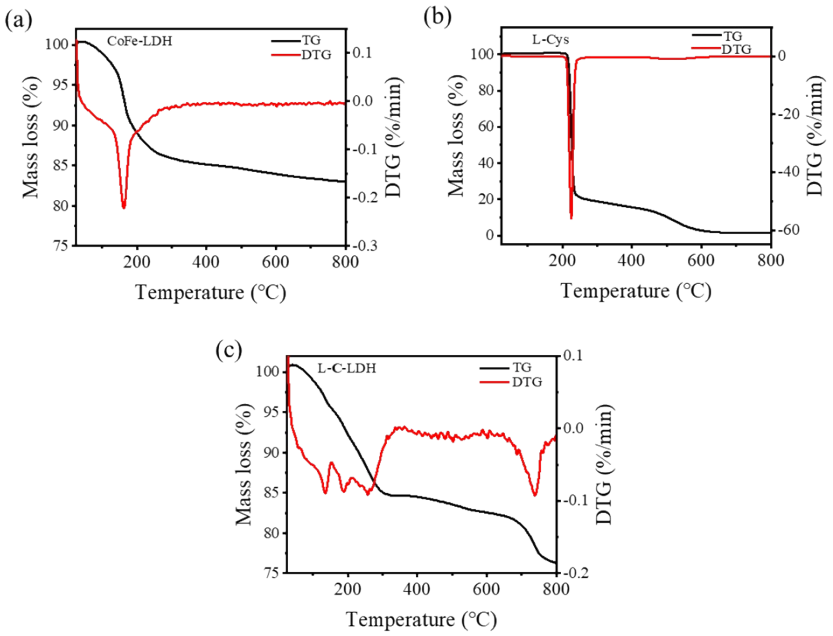

Figure S4. TG-DTA analysis of (a) CoFe-LDH nanozyme, (b) free L-Cys and (c) L-**C**-LDH nanozyme.

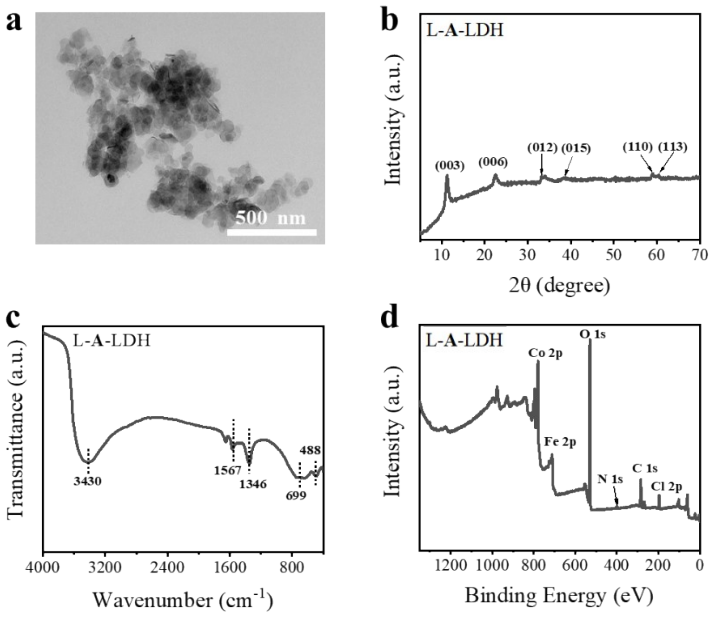

Figure S5. (a) TEM image, (b) PXRD pattern, (c) FT-IR spectrum and (d) XPS survey spectrum of L-**A**-LDH nanozyme.

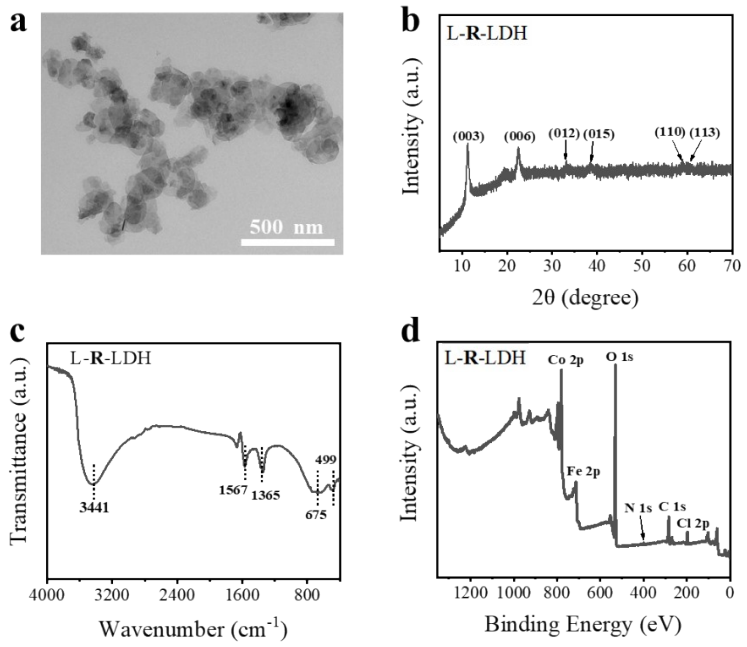

Figure S6. (a) TEM image, (b) PXRD pattern, (c) FT-IR spectrum and (d) XPS survey spectrum of L-**R**-LDH nanozyme.

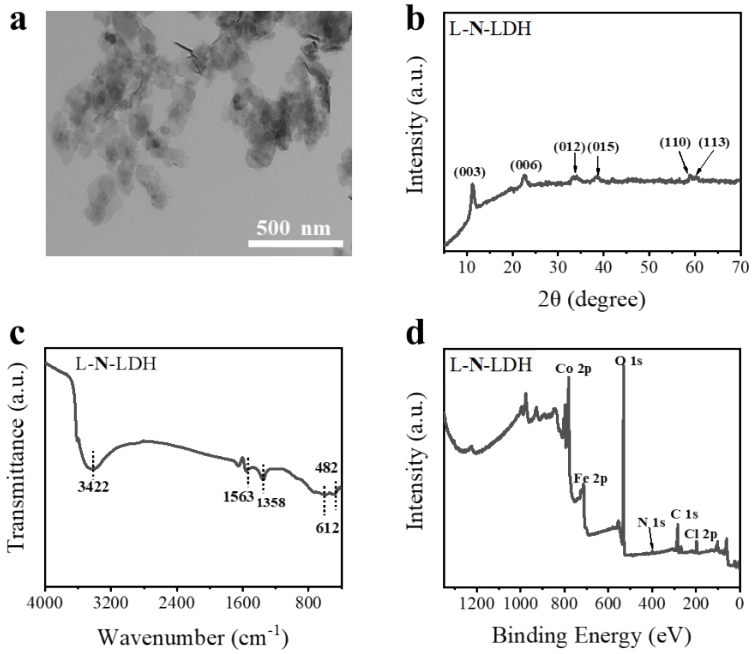

Figure S7. (a) TEM image, (b) PXRD pattern, (c) FT-IR spectrum and (d) XPS survey spectrum of L-**N**-LDH nanozyme.

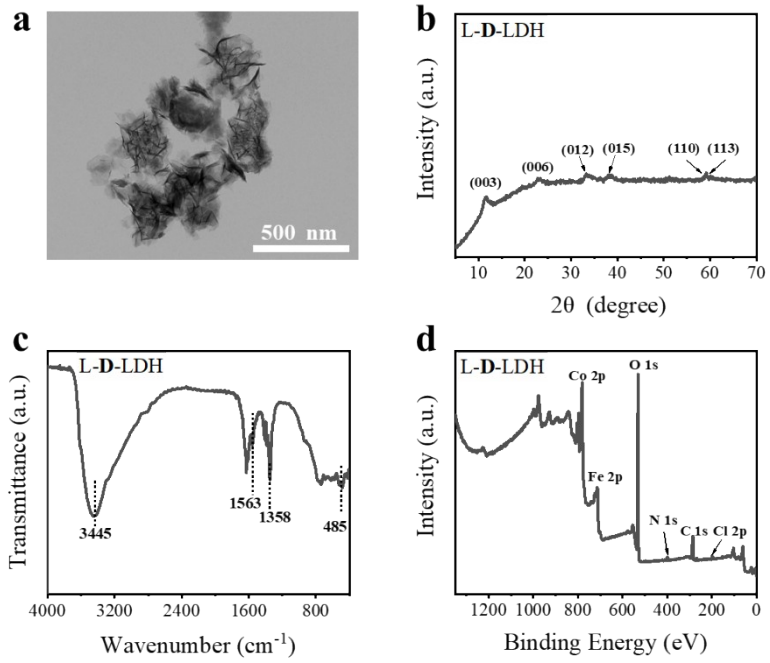

Figure S8. (a) TEM image, (b) PXRD pattern, (c) FT-IR spectrum and (d) XPS survey spectrum of L-**D**-LDH nanozyme.

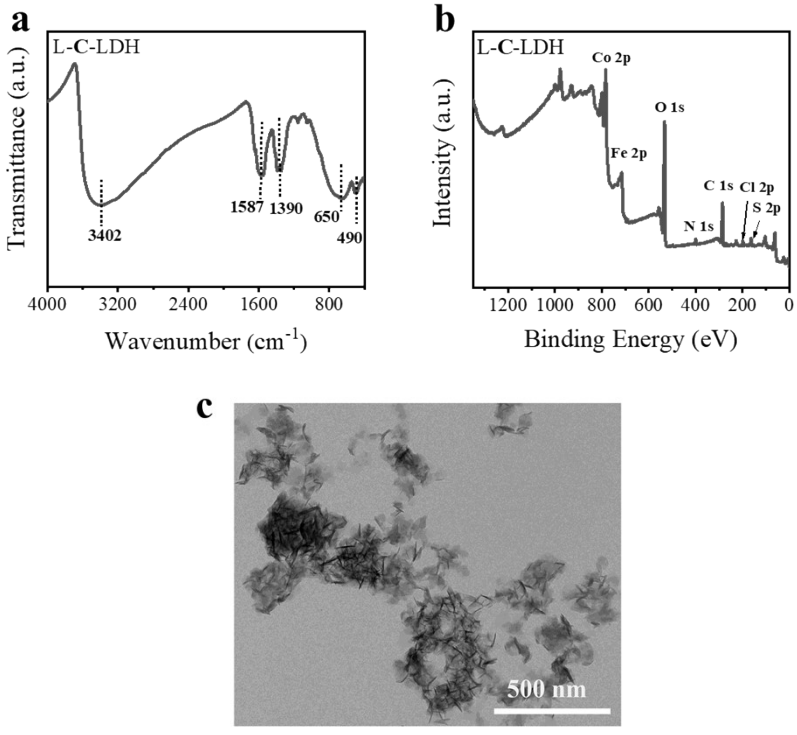

Figure S9. (a) FT-IR spectrum, (b) XPS survey spectrum and (c) TEM image of L-**C**-LDH nanozyme.

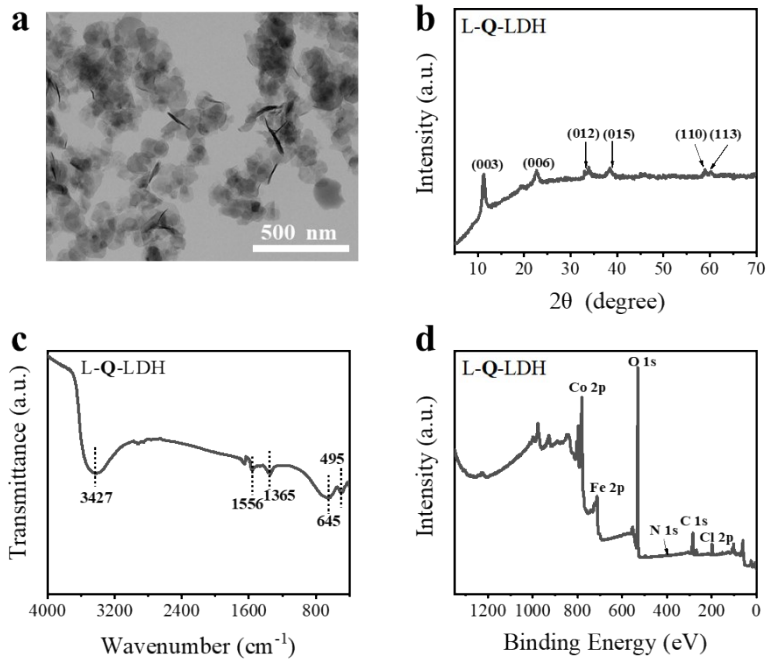

Figure S10. (a) TEM image, (b) PXRD pattern, (c) FT-IR spectrum and (d) XPS survey spectrum of L-**Q**-LDH nanozyme.

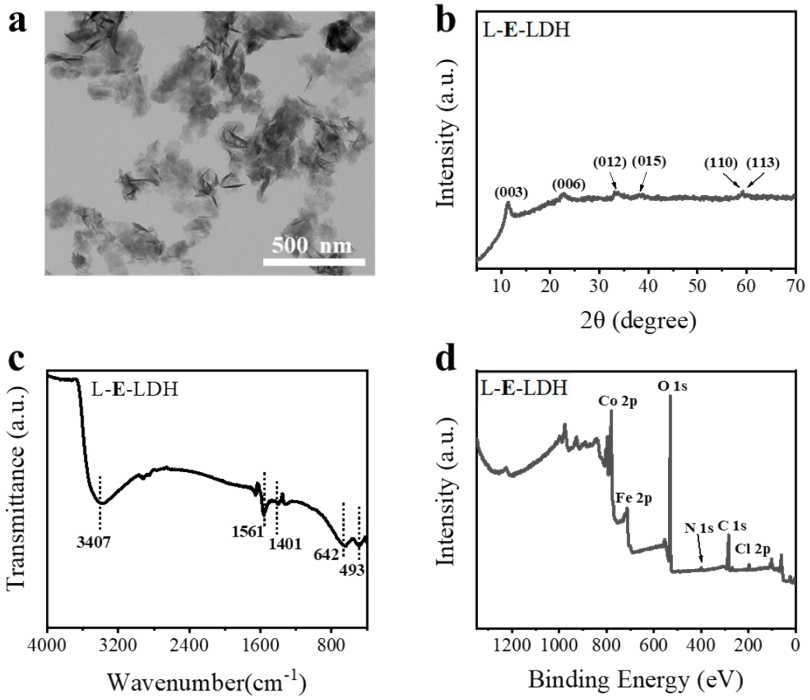

Figure S11. (a) TEM image, (b) PXRD pattern, (c) FT-IR spectrum and (d) XPS survey spectrum of L-**E**-LDH nanozyme.

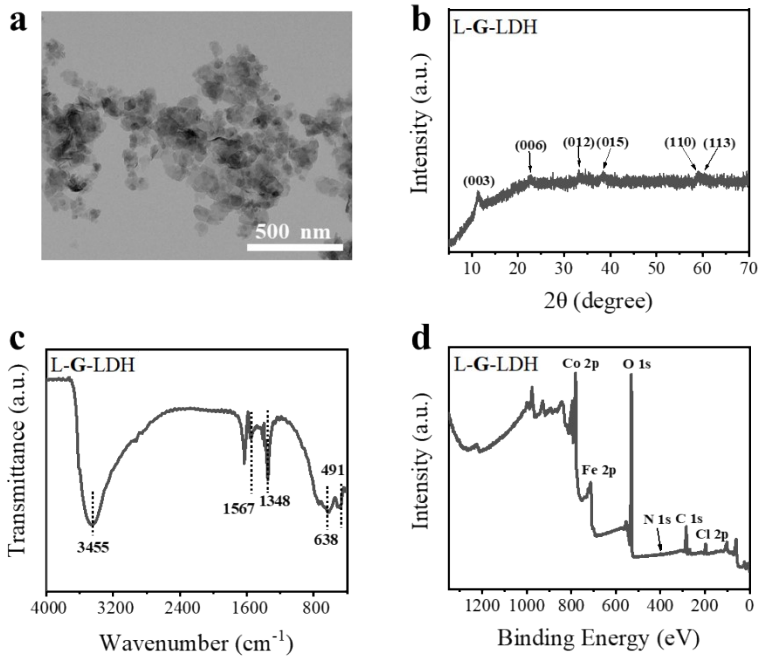

Figure S12. (a) TEM image, (b) PXRD pattern, (c) FT-IR spectrum and (d) XPS survey spectrum of L-**G**-LDH nanozyme.

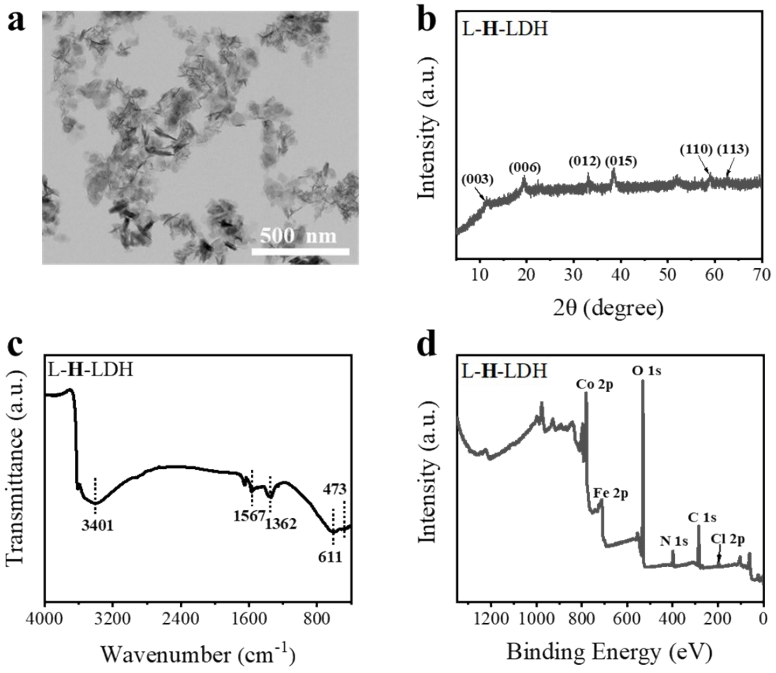

Figure S13. (a) TEM image, (b) PXRD pattern, (c) FT-IR spectrum and (d) XPS survey spectrum of L-**H**-LDH nanozyme.

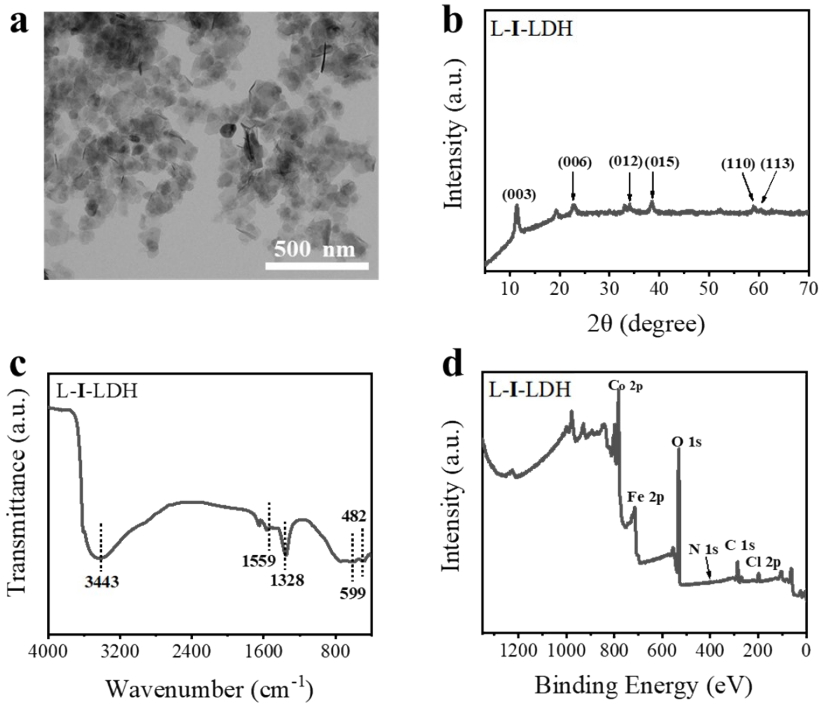

Figure S14. (a) TEM image, (b) PXRD pattern, (c) FT-IR spectrum and (d) XPS survey spectrum of L-**I**-LDH nanozyme.

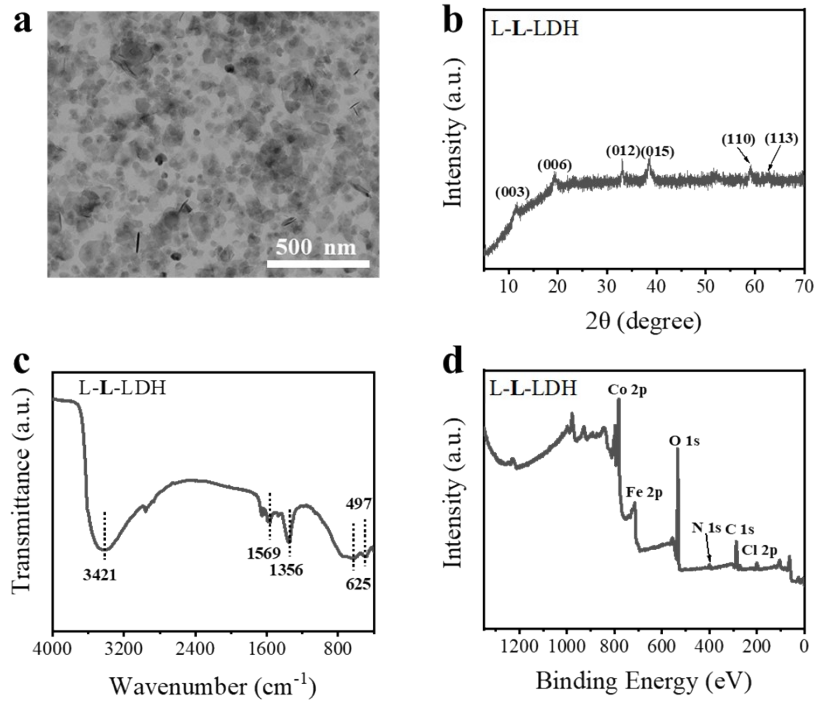

Figure S15. (a) TEM image, (b) PXRD pattern, (c) FT-IR spectrum and (d) XPS survey spectrum of L-**L**-LDH nanozyme.

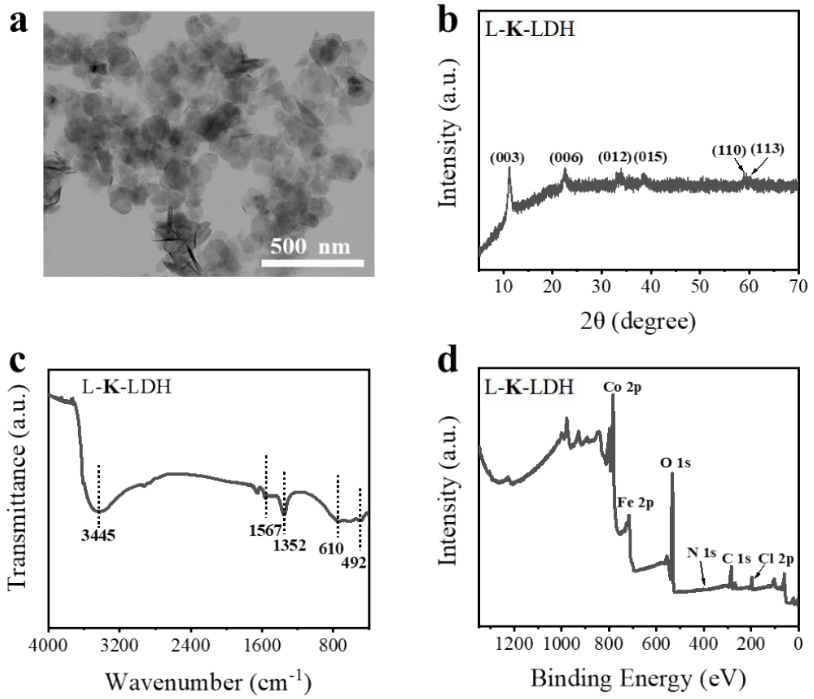

Figure S16. (a) TEM image, (b) PXRD pattern, (c) FT-IR spectrum and (d) XPS survey spectrum of L-**K**-LDH nanozyme.

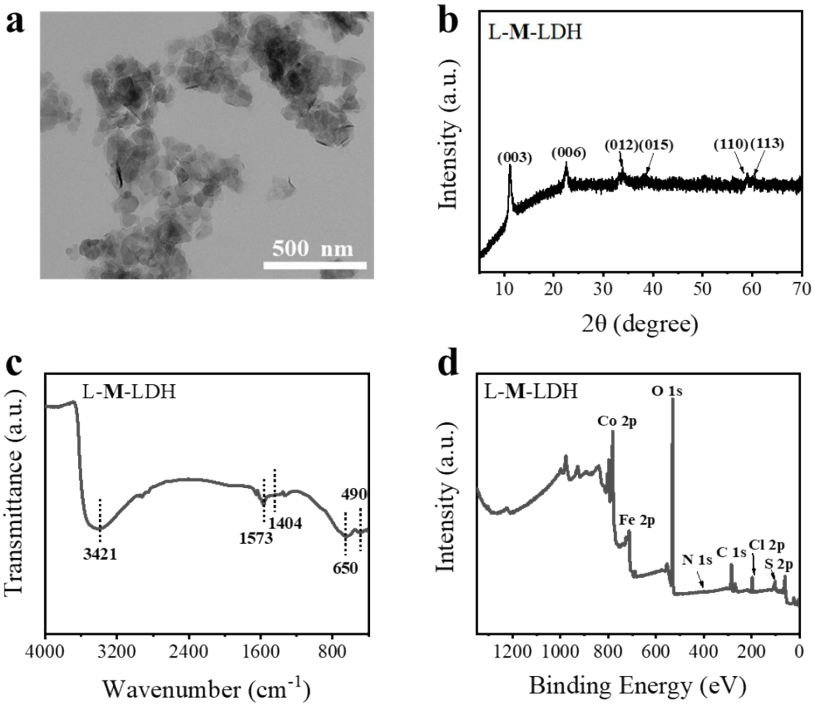

Figure S17. (a) TEM image, (b) PXRD pattern, (c) FT-IR spectrum and (d) XPS survey spectrum of L-**M**-LDH nanozyme.

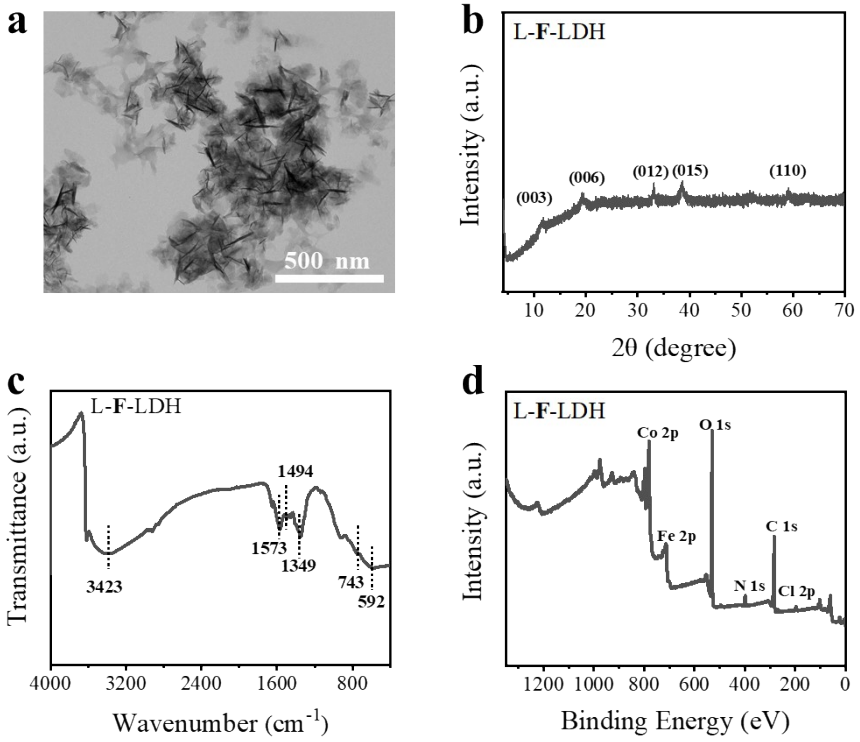

Figure S18. (a) TEM image, (b) PXRD pattern, (c) FT-IR spectrum and (d) XPS survey spectrum of L-**F**-LDH nanozyme.

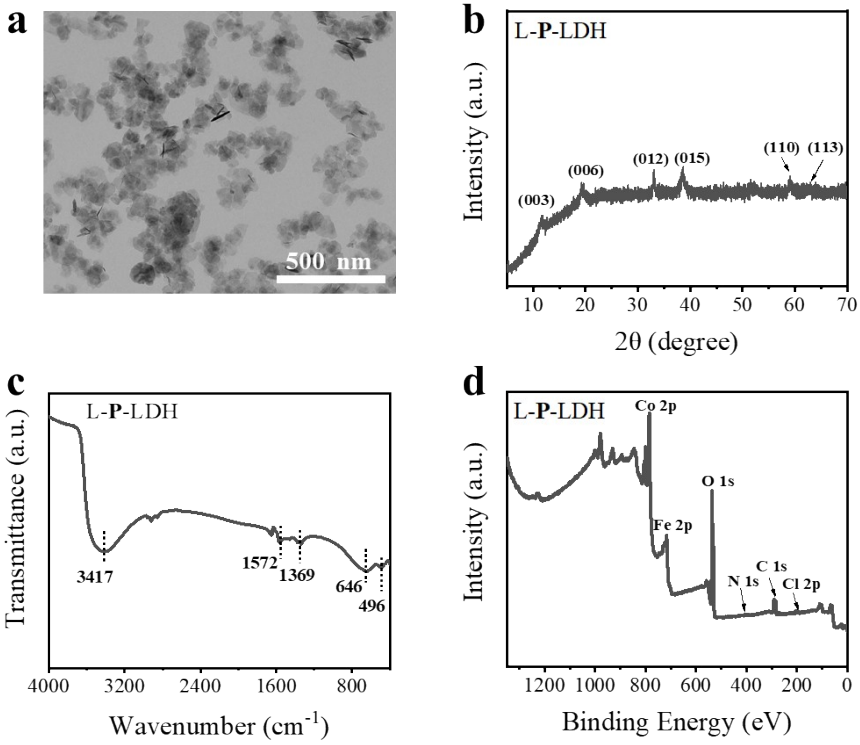

Figure S19. (a) TEM image, (b) PXRD pattern, (c) FT-IR spectrum and (d) XPS survey spectrum of L-**P**-LDH nanozyme.

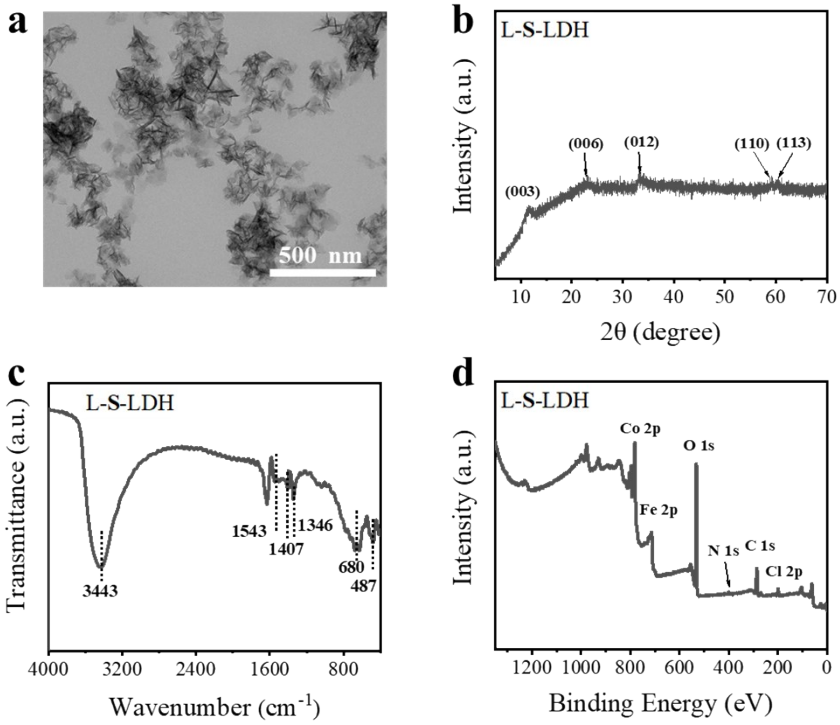

Figure S20. (a) TEM image, (b) PXRD pattern, (c) FT-IR spectrum and (d) XPS survey spectrum of L-**S**-LDH nanozyme.

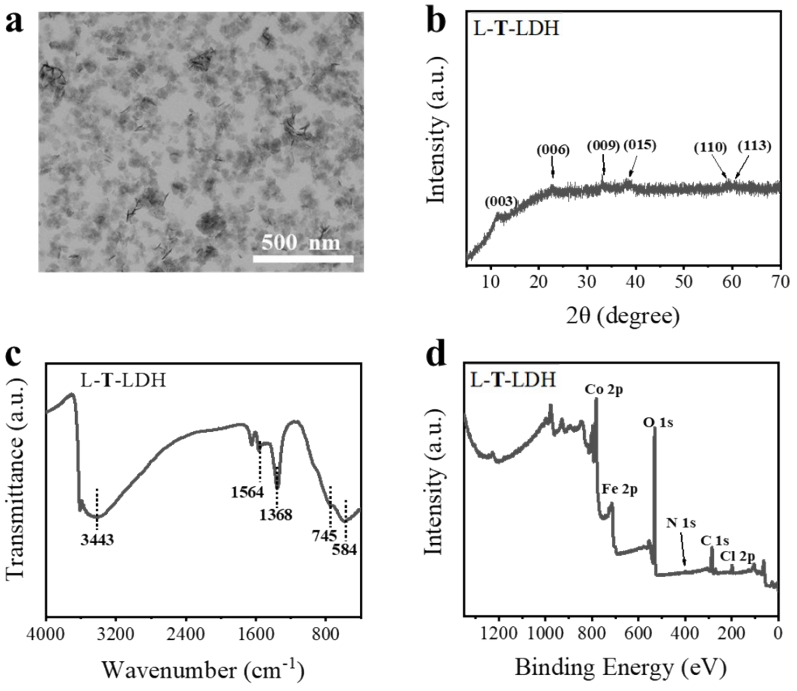

Figure S21. (a) TEM image, (b) PXRD pattern, (c) FT-IR spectrum and (d) XPS survey spectrum of L-**T**-LDH nanozyme.

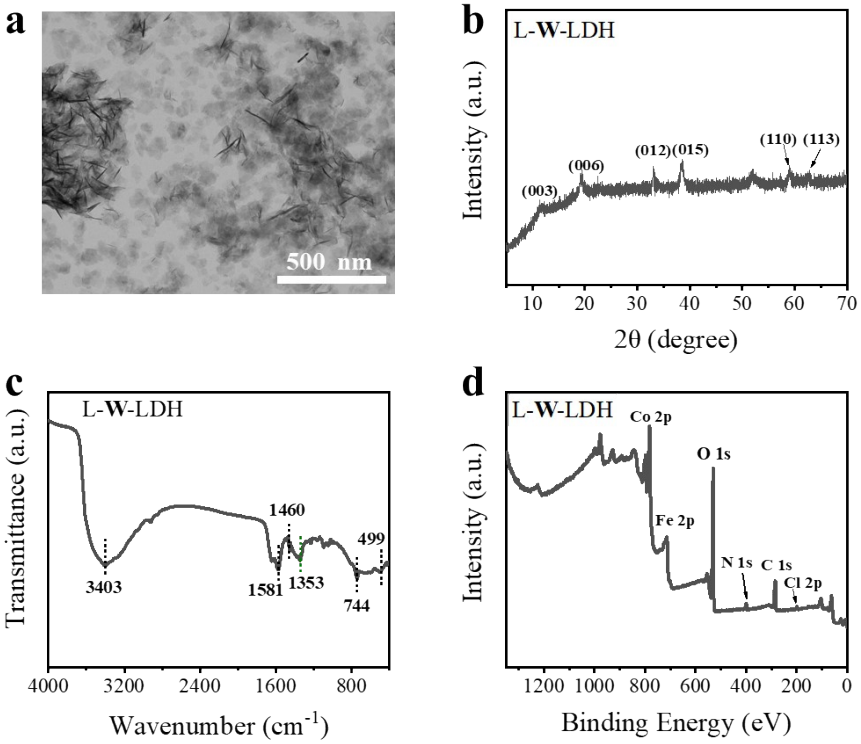

Figure S22. (a) TEM image, (b) PXRD pattern, (c) FT-IR spectrum and (d) XPS survey spectrum of L-**W**-LDH nanozyme.

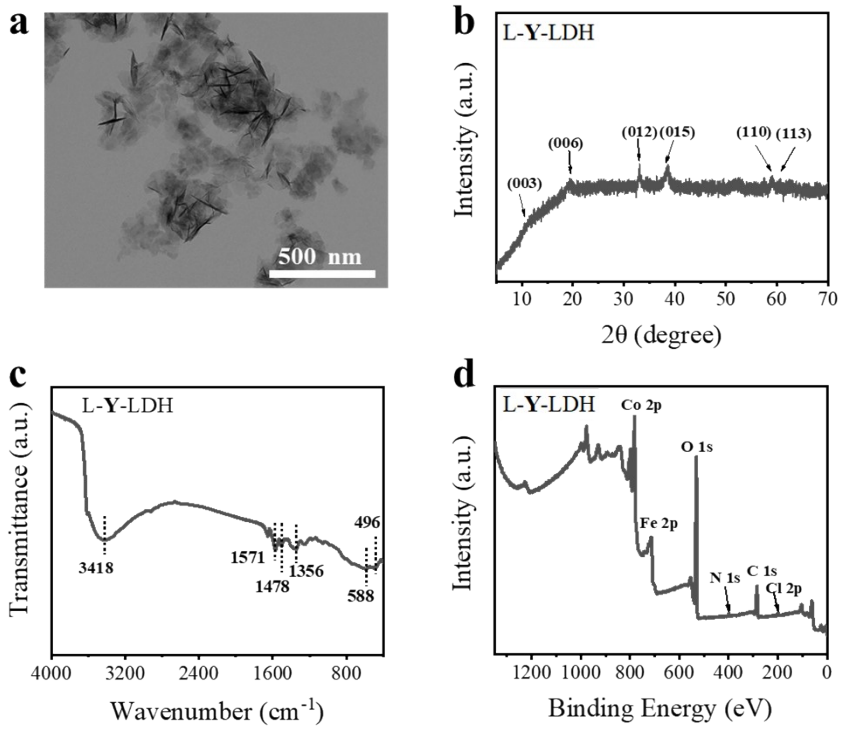

Figure S23. (a) TEM image, (b) PXRD pattern, (c) FT-IR spectrum and (d) XPS survey spectrum of L-**Y**-LDH nanozyme.

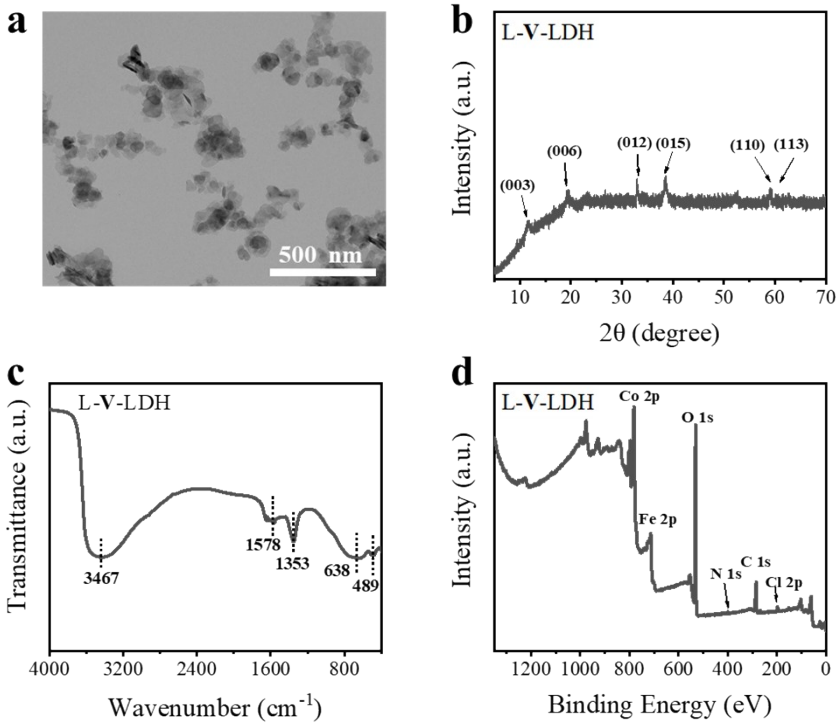

Figure S24. (a) TEM image, (b) PXRD pattern, (c) FT-IR spectrum and (d) XPS survey spectrum of L-**V**-LDH nanozyme.

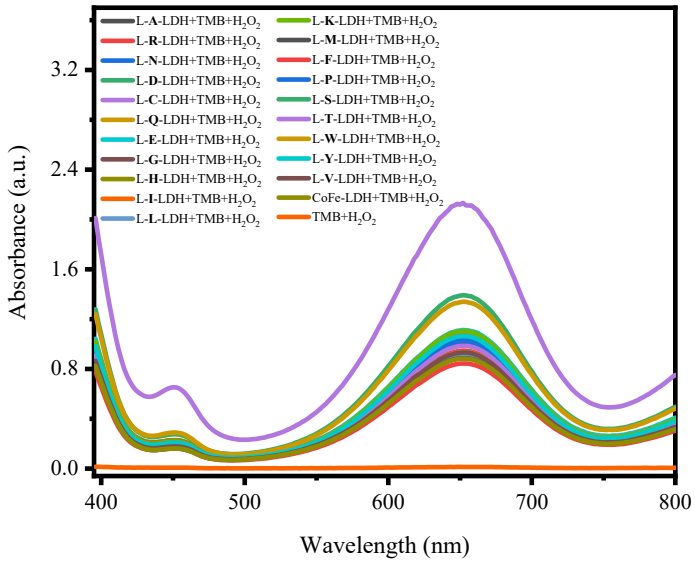

Figure S25. The UV-visible spectra of the catalytic systems based on CoFe-LDH nanozyme and different L-AA-LDH nanozymes. Reaction conditions: L-AA-LDH (10 μg mL^{-1}), TMB (0.2 mM) and H_2O_2 (0.2 mM) were added in 0.2 M acetate buffer (pH = 3.0) and incubated at room temperature for 10 min. Error bar showed the standard deviation of three independent measurements.

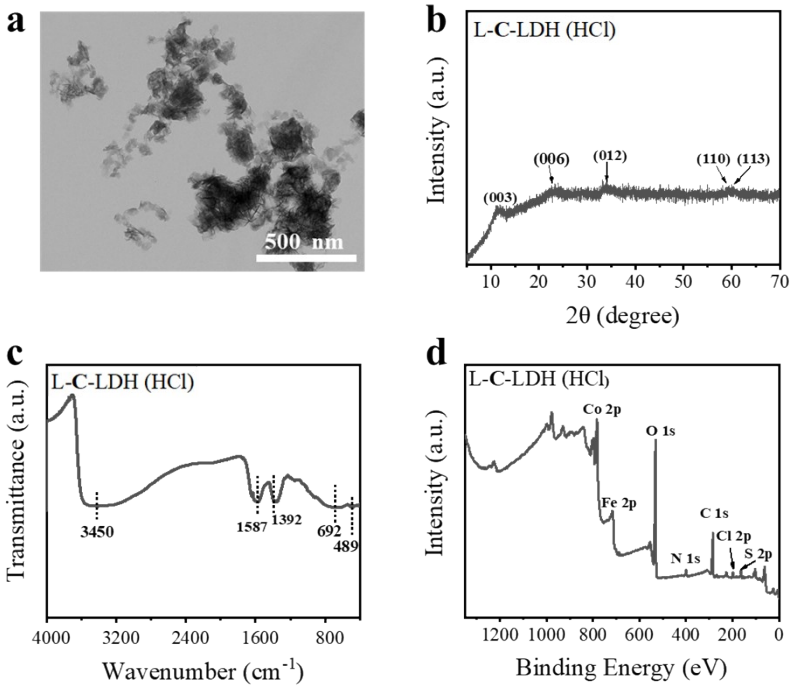

Figure S26. (a) TEM image, (b) PXRD pattern, (c) FT-IR spectrum and (d) XPS survey spectrum of L-**C**-LDH nanozyme (HCl).

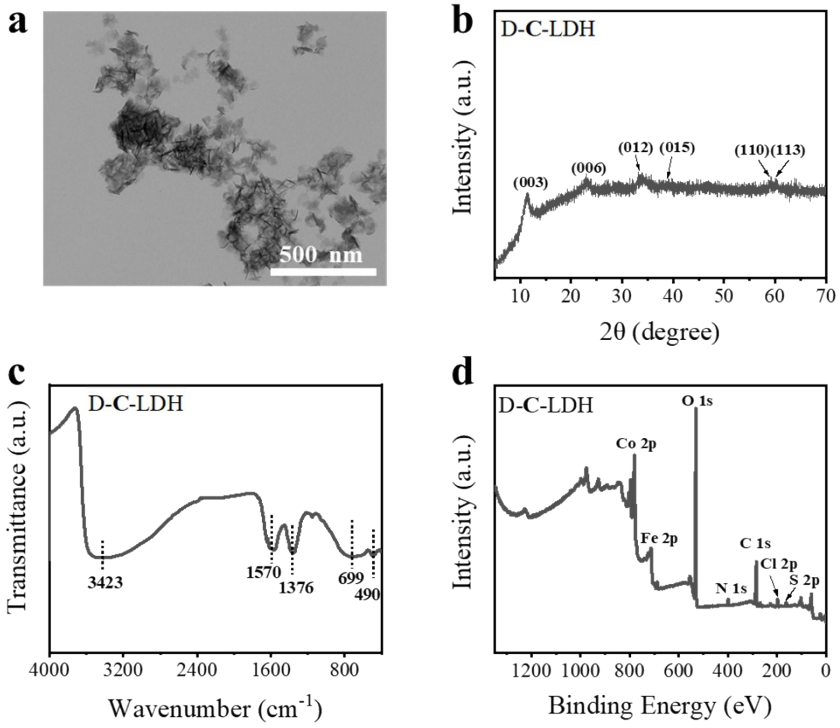

Figure S27. (a) TEM image, (b) PXRD pattern, (c) FT-IR spectrum and (d) XPS survey spectrum of D-**C**-LDH nanozyme.

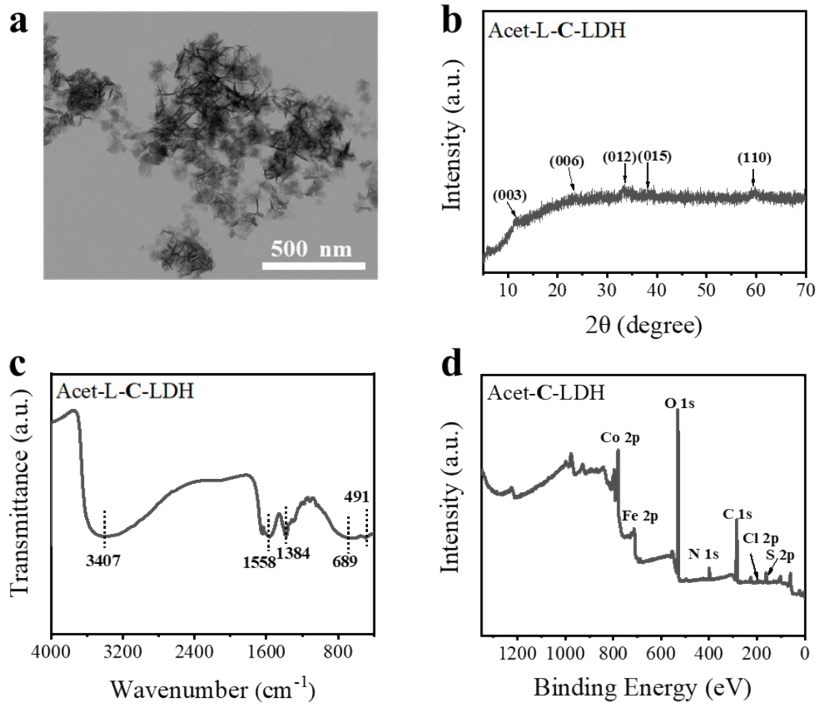

Figure S28. (a) TEM image, (b) PXRD pattern, (c) FT-IR spectrum and (d) XPS survey spectrum of Acet-L-**C**-LDH nanozyme.

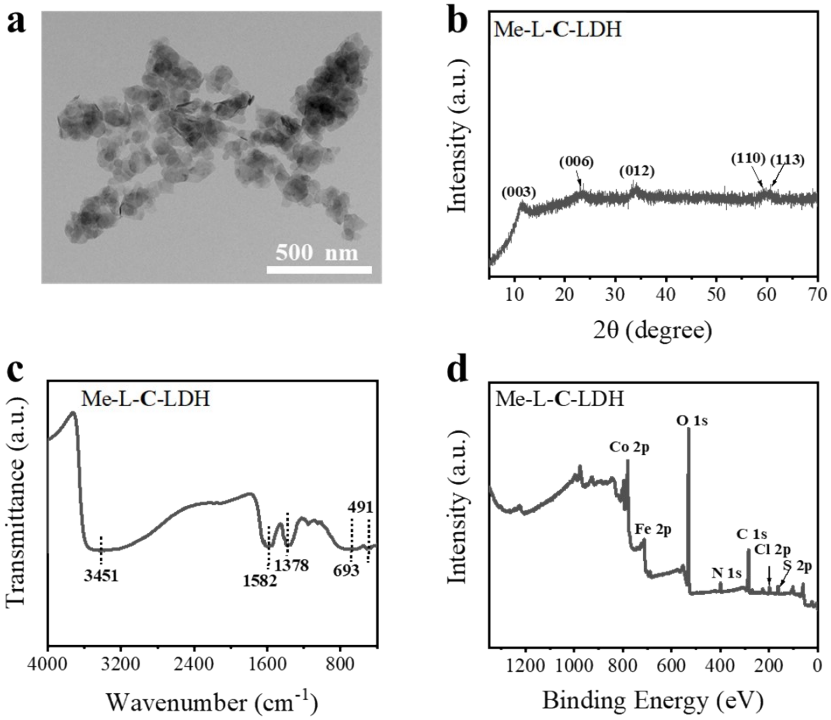

Figure S29. (a) TEM image, (b) PXRD pattern, (c) FT-IR spectrum and (d) XPS survey spectrum of Me-L-**C**-LDH nanozyme.

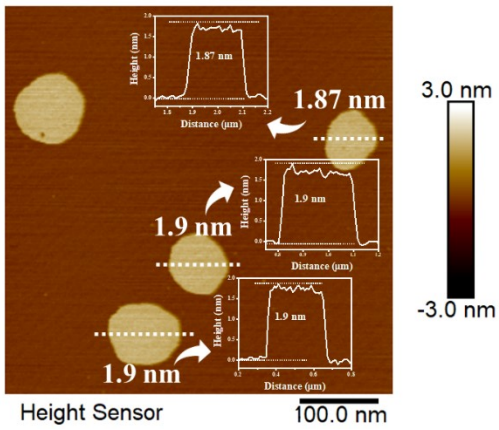

Figure S30. AFM image of Me-L-**C**-LDH nanozyme.

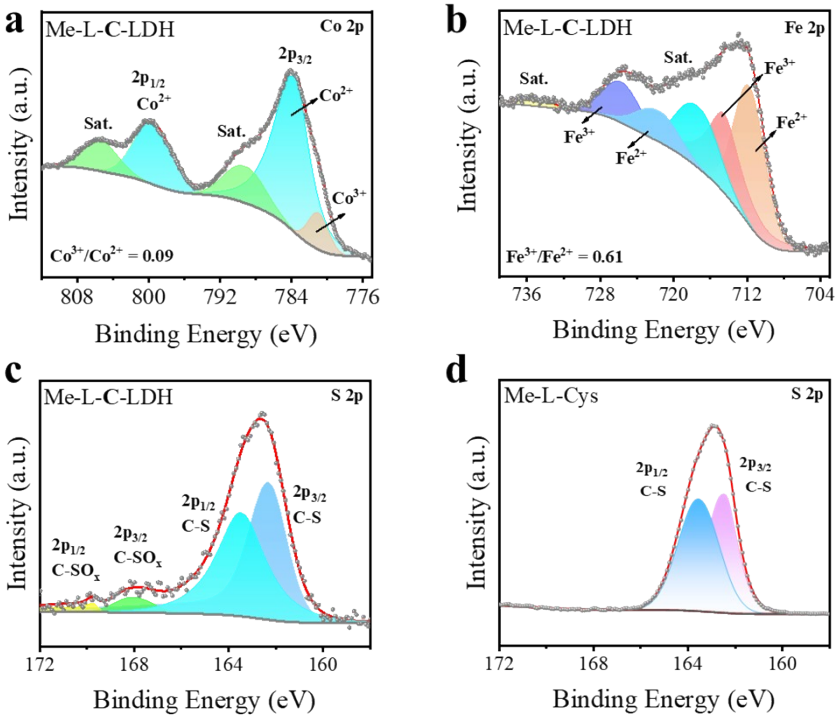

Figure S31. (a) Co 2p, (b) Fe 2p and (c) S 2p XPS spectrum of Me-L-**C**-LDH nanozyme. (d) S 2p XPS spectrum of Me-L-Cys.

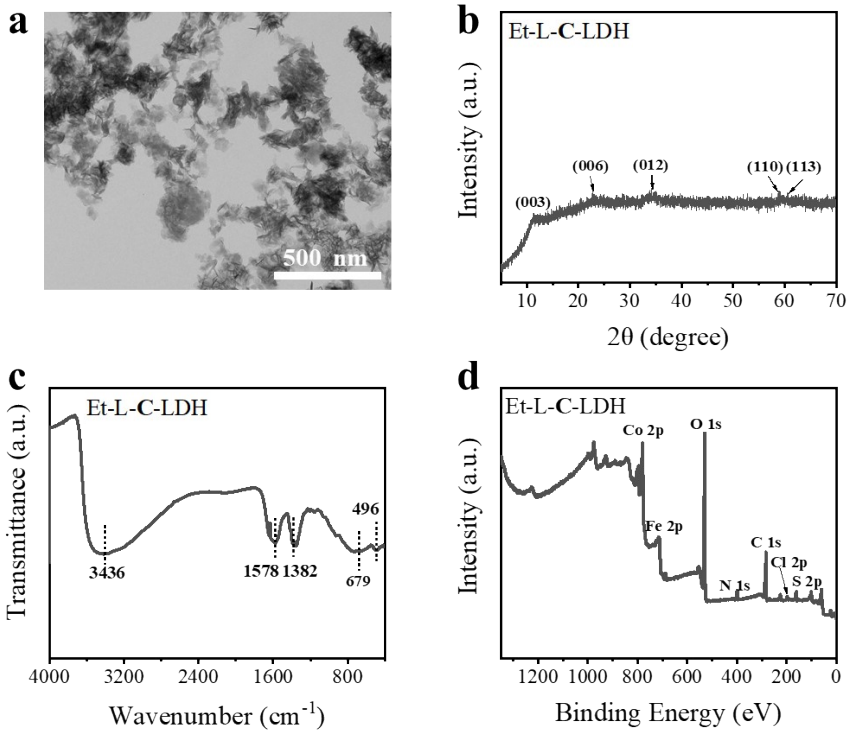

Figure S32. (a) TEM image, (b) PXRD pattern, (c) FT-IR spectrum and (d) XPS survey spectrum of Et-L-**C**-LDH nanozyme.

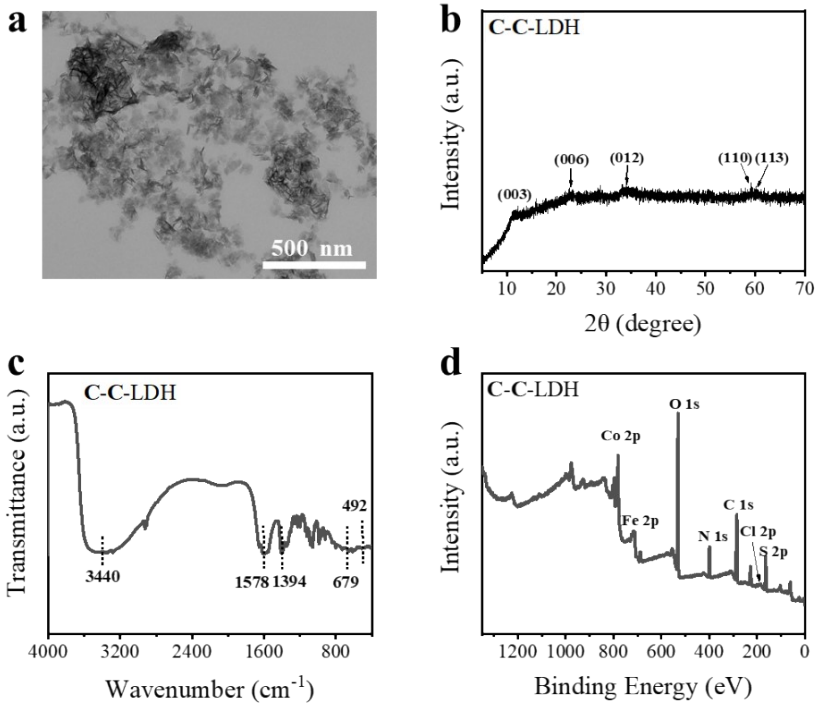

Figure S33. (a) TEM image, (b) PXRD pattern, (c) FT-IR spectrum and (d) XPS survey spectrum of **C**-**C**-LDH nanozyme.

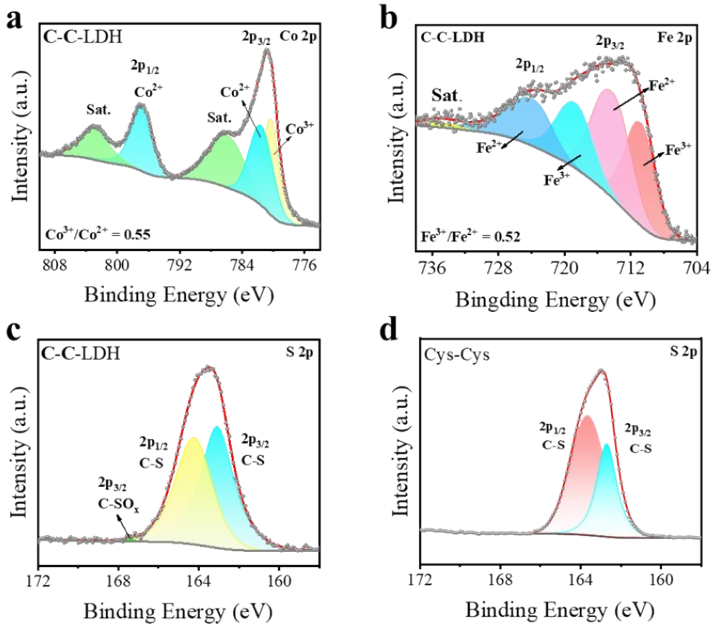

Figure S34. (a) Co 2p, (b) Fe 2p and (c) S 2p XPS spectrum of **C-C**-LDH nanozyme. (d) S 2p XPS spectrum of Cys-Cys.

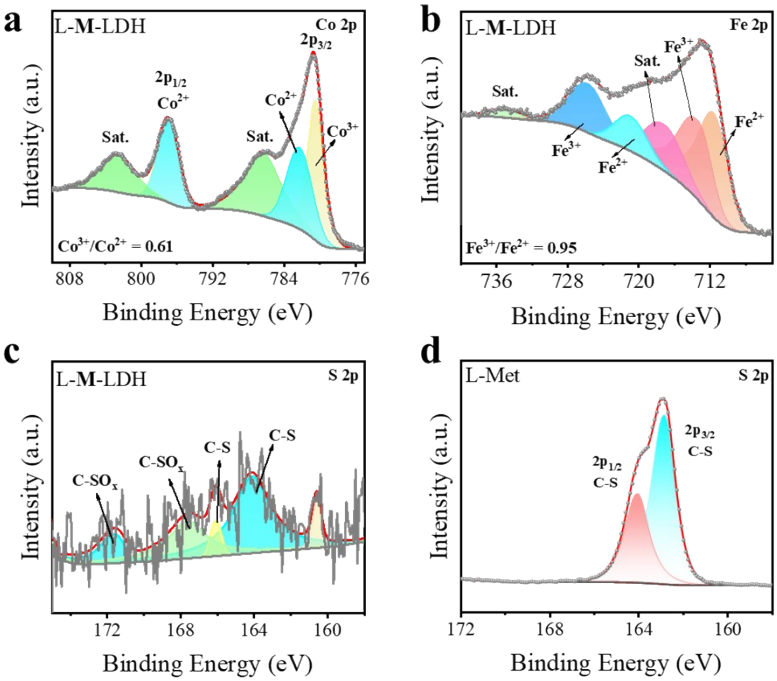

Figure S35. (a) Co 2p, (b) Fe 2p and (c) S 2p XPS spectrum of L-**M**-LDH nanozyme. (d) S 2p XPS spectrum of L-Met.

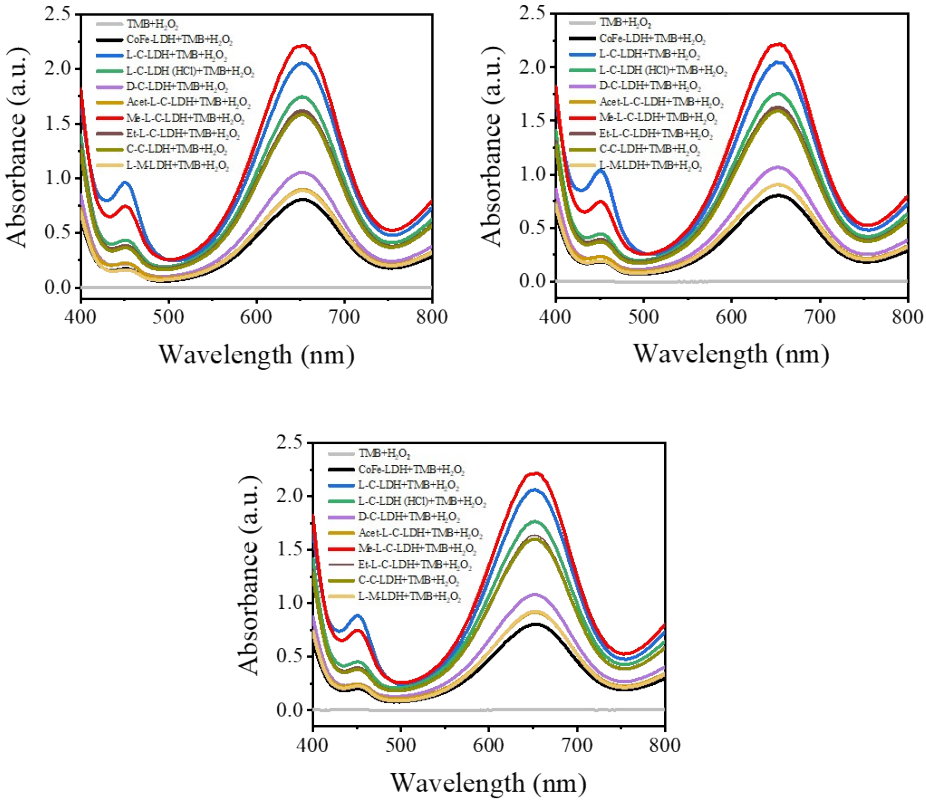

Figure S36. The UV-visible spectra of the catalytic systems based on CoFe-LDH nanozyme and different **C**-LDH nanozymes. Reaction conditions: **C**-LDH nanozyme (10 μg mL^{-1}), TMB (0.2 mM) and H_2O_2 (0.2 mM) were added in 0.2 M acetate buffer (pH = 3.0) and incubated at room temperature for 10 min.

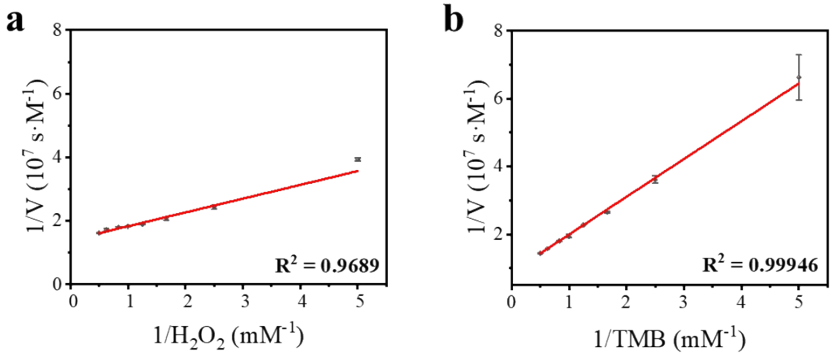

Figure S37. The corresponding double-reciprocal plot of CoFe-LDH with varied concentrations of (a) H_2O_2 and (b) TMB at 37°C.

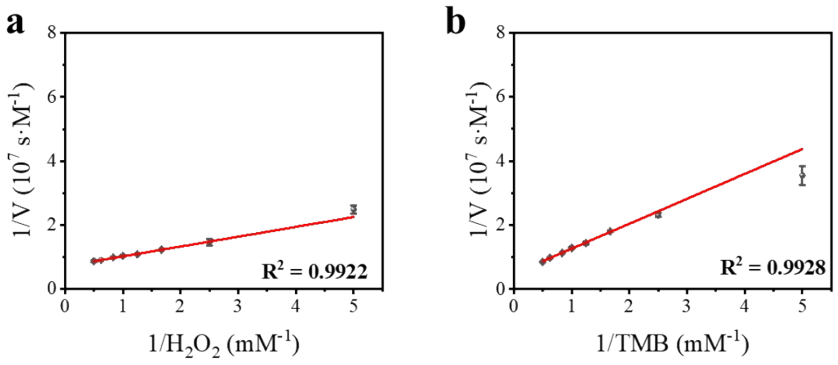

Figure S38. The corresponding double-reciprocal plot of L-**C**-LDH nanozyme with varied concentrations of (a) H_2O_2 and (b) TMB at 37°C.

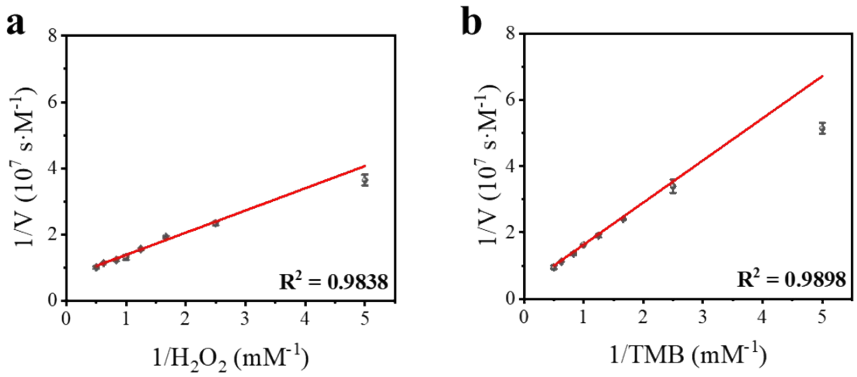

Figure S39. The corresponding double-reciprocal plot of Me-L-**C**-LDH nanozyme with varied concentrations of (a) H_2O_2 and (b) TMB at 37°C.

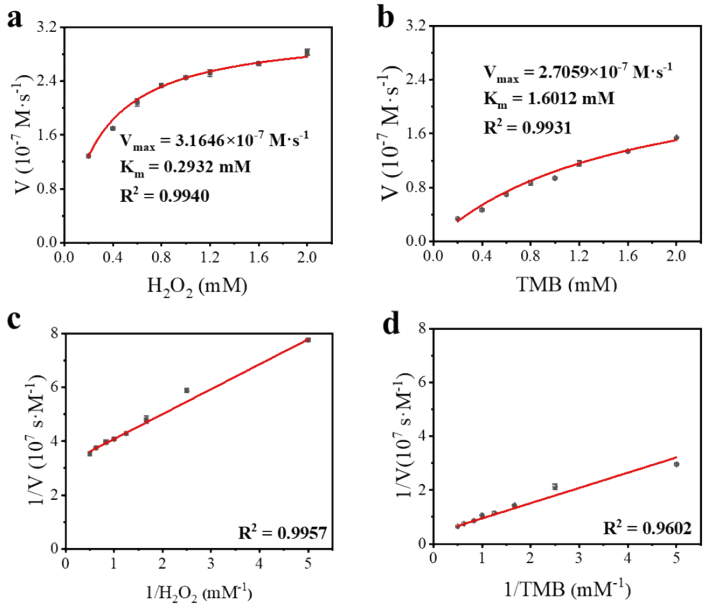

Figure S40. Steady-state kinetic curve of CoFe-LDH nanozyme with varied concentrations of (a) H_2O_2 and (b) TMB. The reaction rate versus H_2O_2 concentration was at a fixed concentration of TMB (1.50 mM). The reaction rate versus TMB concentration was at a fixed concentration of H_2O_2 (1.50 mM). The corresponding double-reciprocal plot of CoFe-LDH nanozyme with varied concentrations of (c) H_2O_2 and (d) TMB at 25°C. Each error bar showed the standard deviation of three independent measurements.

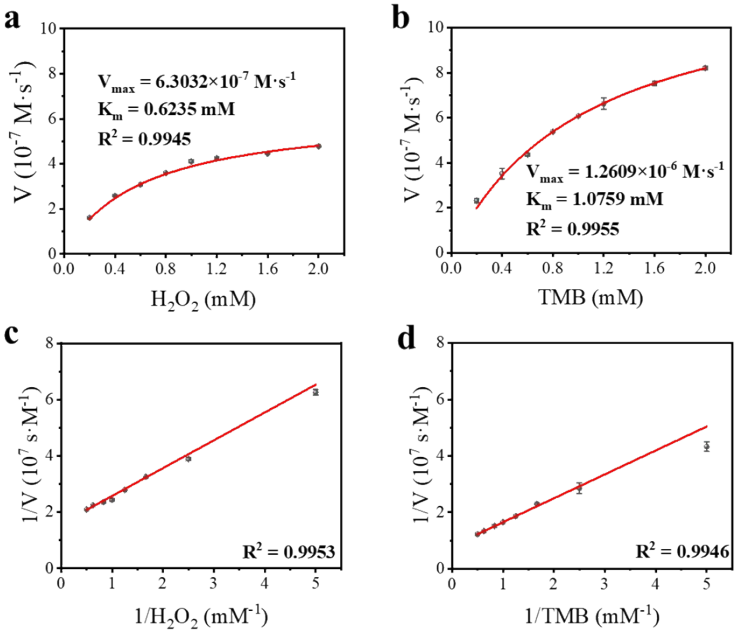

Figure S41. Steady-state kinetic curve of L-**C**-LDH nanozyme with varied concentrations of (a) H_2O_2 and (b) TMB. The reaction rate versus H_2O_2 concentration was at a fixed concentration of TMB (1.50 mM). The reaction rate versus TMB concentration was at a fixed concentration of H_2O_2 (1.50 mM). The corresponding double-reciprocal plot of L-**C**-LDH nanozyme with varied concentrations of (c) H_2O_2 and (d) TMB at 25°C. Each error bar showed the standard deviation of three independent measurements.

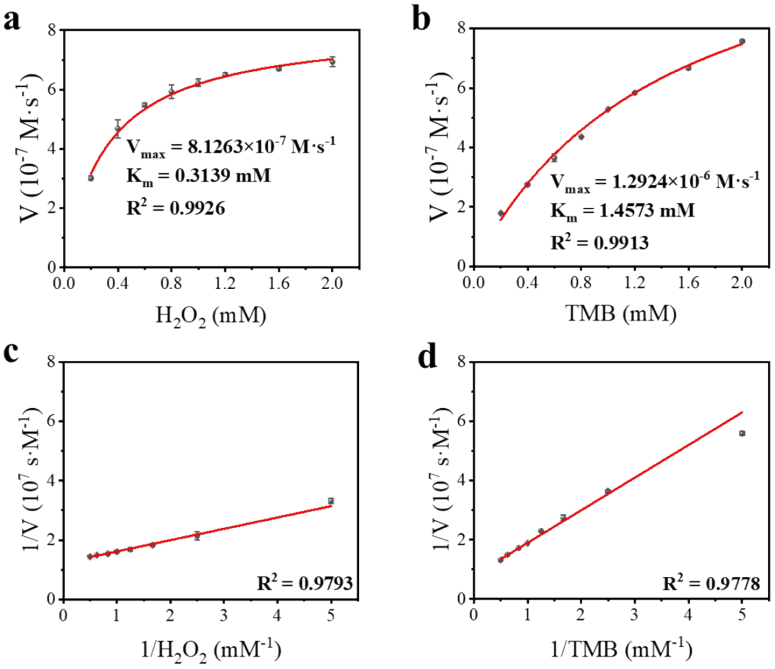

Figure S42. Steady-state kinetic curve of Me-L-**C**-LDH nanozyme with varied concentrations of (a) H_2O_2 and (b) TMB. The reaction rate versus H_2O_2 concentration was at a fixed concentration of TMB (1.50 mM). The reaction rate versus TMB concentration was at a fixed concentration of H_2O_2 (1.50 mM). The corresponding double-reciprocal plot of Me-L-**C**-LDH nanozyme with varied concentrations of (c) H_2O_2 and (d) TMB at 25°C. Each error bar showed the standard deviation of three independent measurements.

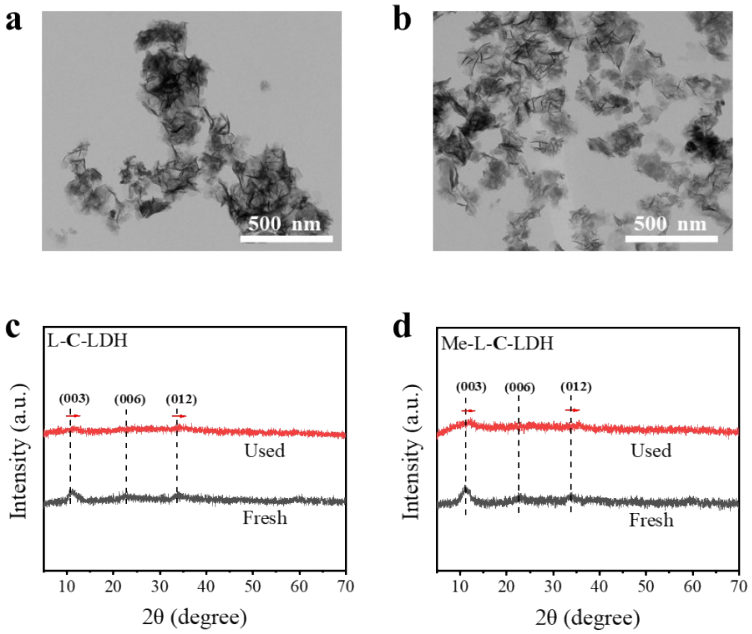

Figure S43. TEM images of (a) L-**C**-LDH nanozyme and (b) Me-L-**C**-LDH nanozyme which has been used. PXRD patterns of (c) L-**C**-LDH nanozyme and (d) Me-L-**C**-LDH nanozyme which has been used and not.

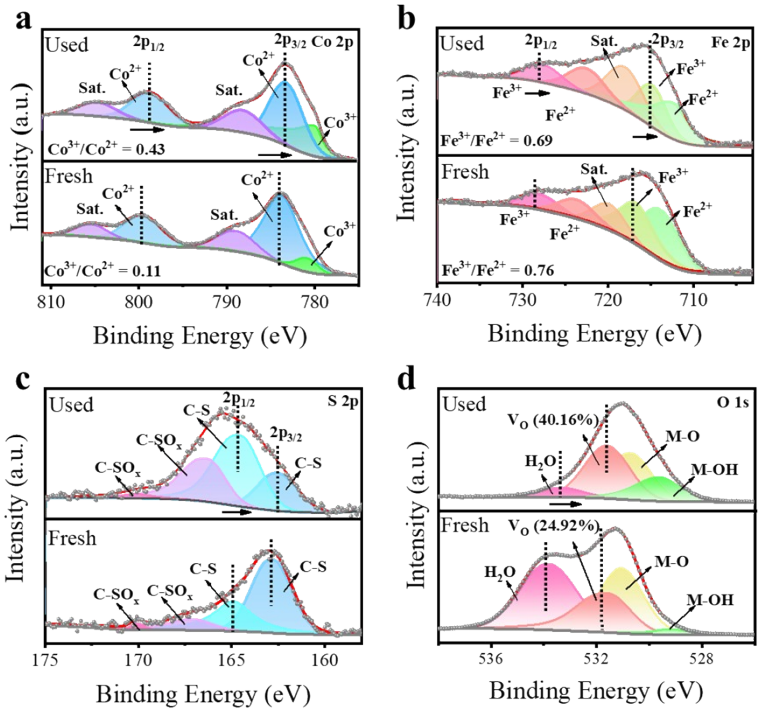

Figure S44. XPS spectra of L-**C**-LDH nanozyme which has been used and not: (a) Co 2p, (b) Fe 2p and (c) S 2p

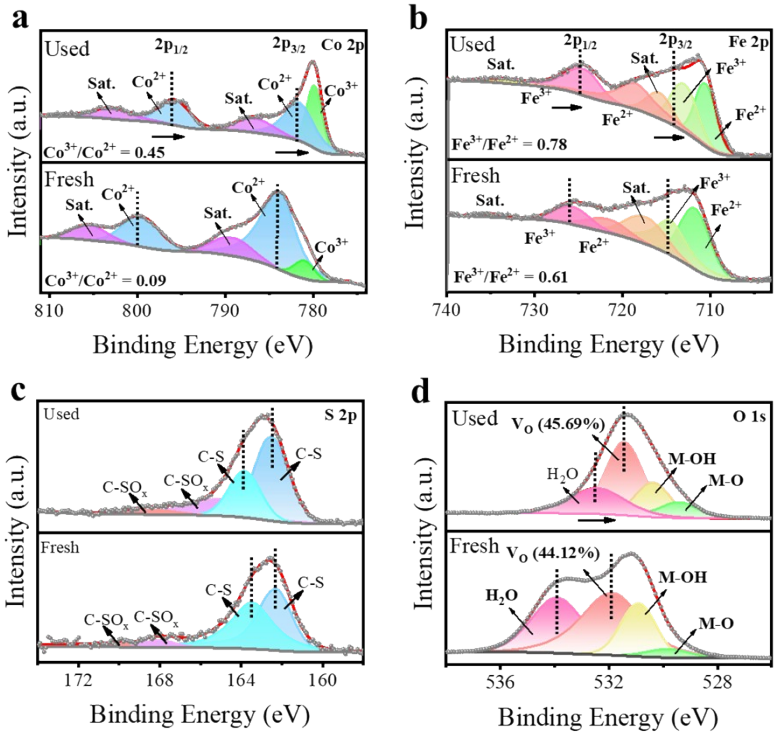

Figure S45. XPS spectra of Me-L-**C**-LDH nanozyme which has been used and not: (a) Co 2p, (b) Fe 2p and (c) S 2p (d) O 1s.

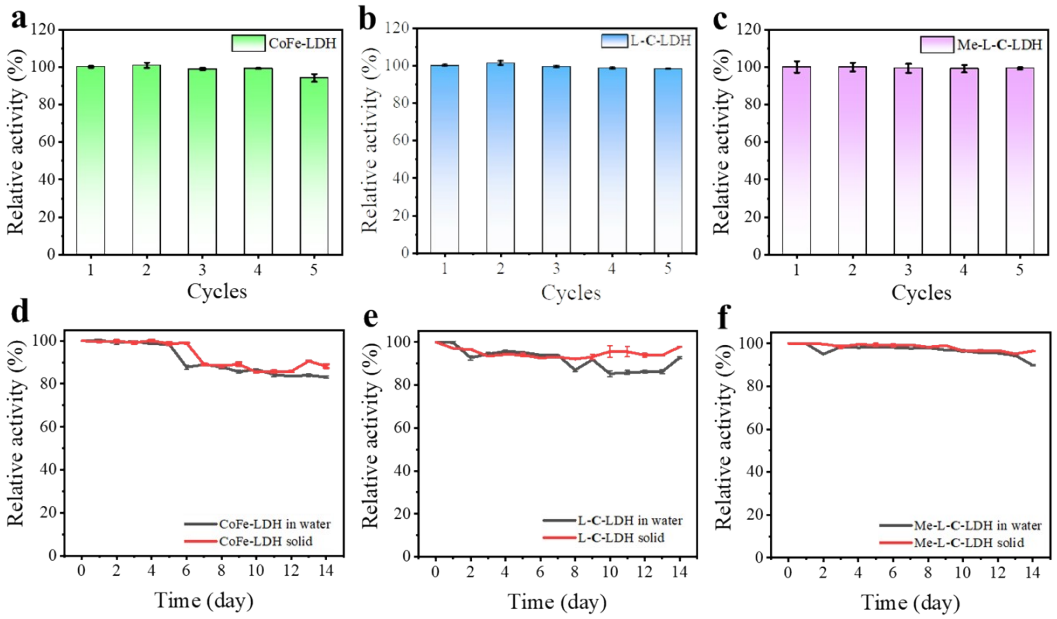

Figure S46. Relative activity changes of (a) CoFe-LDH nanozyme, (b) L-**C**-LDH nanozyme and (c) Me-L-**C**-LDH nanozyme in 5 repeated experiments. Relative activity changes of (c) CoFe-LDH nanozyme, (d) L-**C**-LDH nanozyme and (e) Me-L-**C**-LDH nanozyme of water or solid state after different days. Error bar showed the standard deviation of three independent measurements.

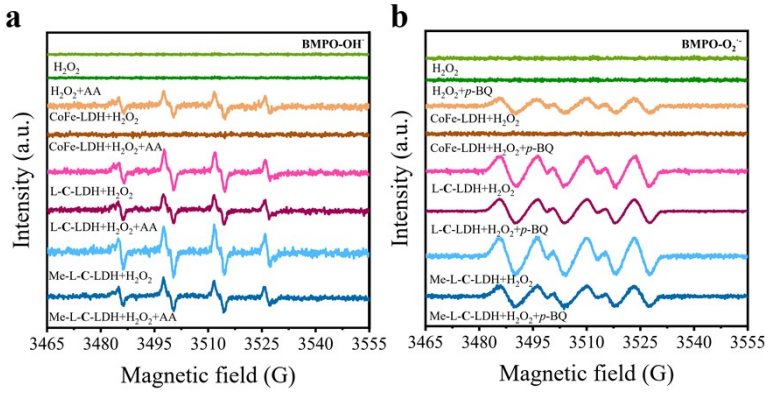

Figure S47. ESR signals of (a) BMPO-·OH adduct and (b) BMPO-·O_2^- adduct in CoFe-LDH/H_2O_2, L-**C**-LDH/H_2O_2 and Me-L-**C**-LDH/H_2O_2 systems.

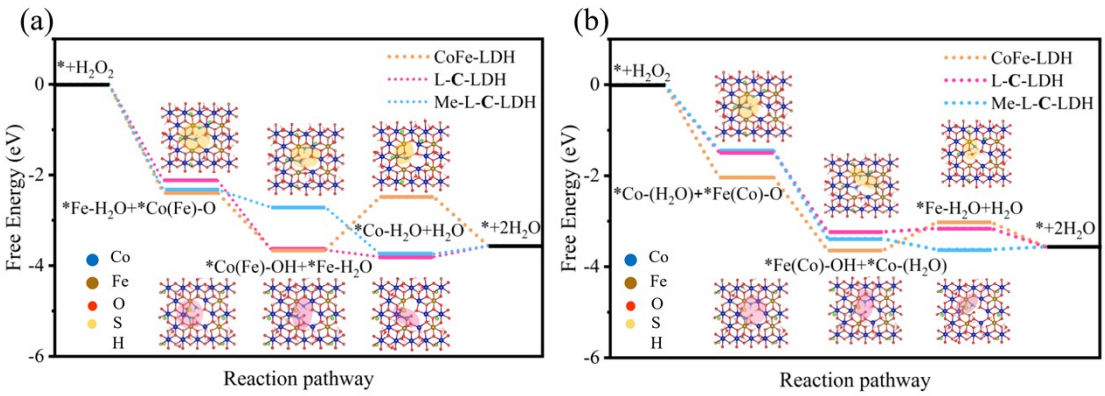

Figure S48. DFT studies on the POD-like activity of LDH nanozymes. The activating process of H_2O_2 by heterolytic path at (a) Fe sites-prior and (b) Co sites-prior. Insets: The catalytic structure modeling of CoFe-LDH nanozyme (yellow) and L-**C**-LDH nanozyme (pink).

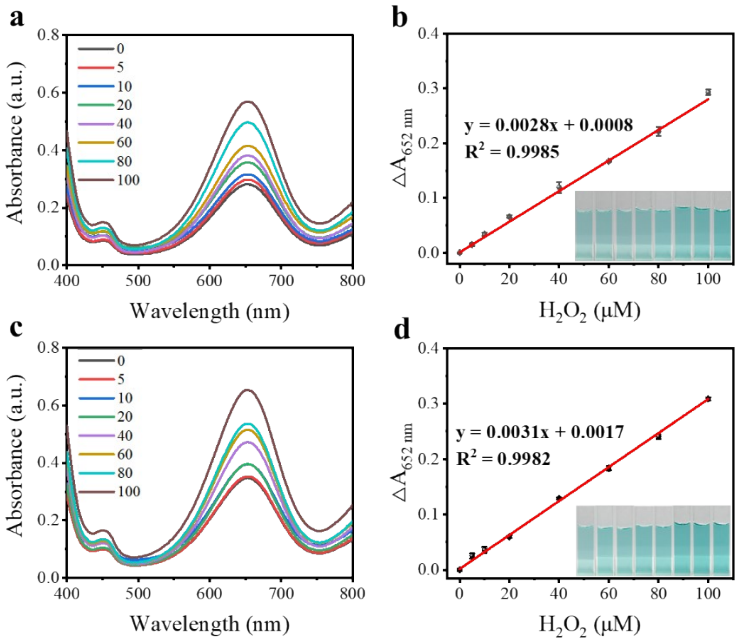

Figure S49. (a) UV-vis spectra of L-**C**-LDH/TMB system upon addition of H_2O_2 with various concentrations: from 5-100 μM. (b) The linear curve between the absorbance at 652 nm and H_2O_2 concentration. (c) UV-vis spectra of Me-L-**C**-LDH/TMB system upon addition of H_2O_2 with various concentrations: from 5-100 μM. (d) The linear curve between the absorbance at 652 nm and H_2O_2 concentration. The inset photograph showed the visually recognizable color change of the reaction systems.

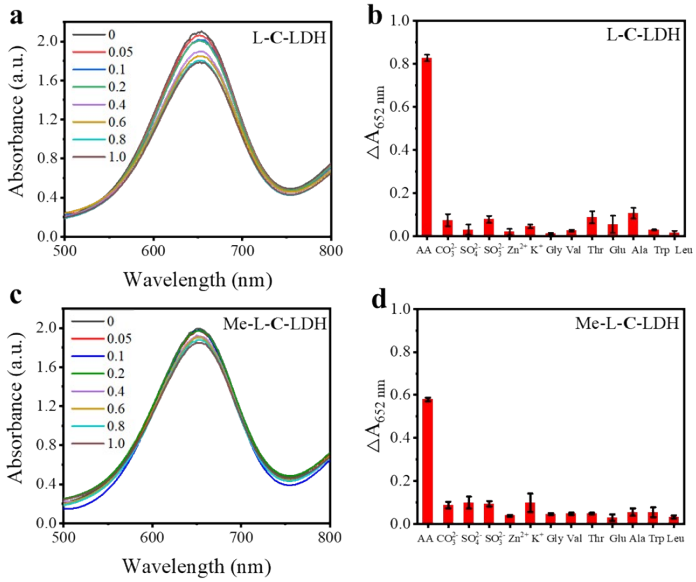

Figure S50. (a) UV-vis spectra of L-**C**-LDH/TMB/H_2O_2 system upon addition of AA with various concentrations: from 0.05-1.0 μM. (c) UV-vis spectra of Me-L-**C**-LDH/TMB/H_2O_2 system upon addition of AA with various concentrations: from 0.05-1.0 μM. Selectivity of (b) L-**C**-LDH nanozyme and (d) Me-L-**C**-LDH nanozyme for the detection of AA. The concentration of AA, interfering ions and amino acids were 60 μM, 500 μM and 100 μM, respectively. The error bar represented the confidence interval for the mean of three measurements.

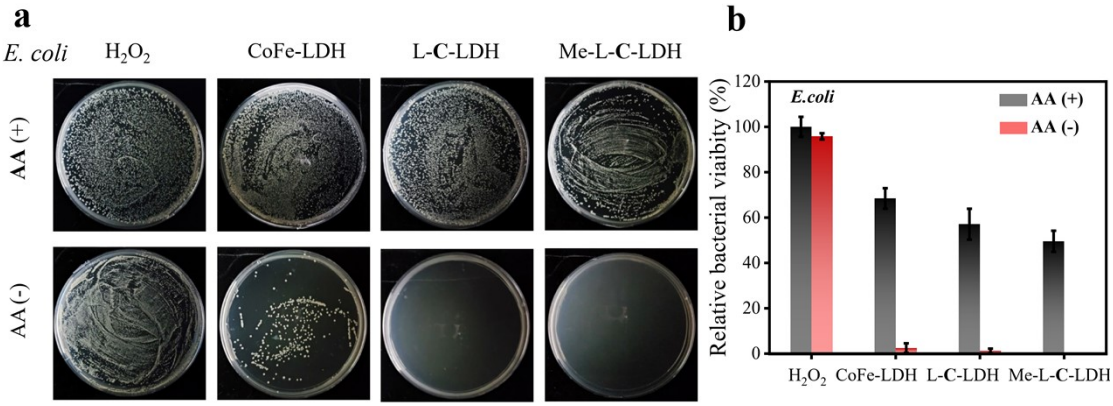

Figure S51. (a) Photograph of bacterial colonies formed by *E. coli* after exposure to control, different nanozymes (CoFe-LDH, L-**C**-LDH and Me-L-**C**-LDH) + H_2O_2 + AA, nanozymes + H_2O_2. The working concentrations for AA, nanozymes, H_2O_2 and sodium acetate buffer were 2 mM, 250 μg mL^{-1}, 1 mM and 0.1 M, respectively. (b) Corresponding bacterial viability measurement of *E. coli* upon different treatments.

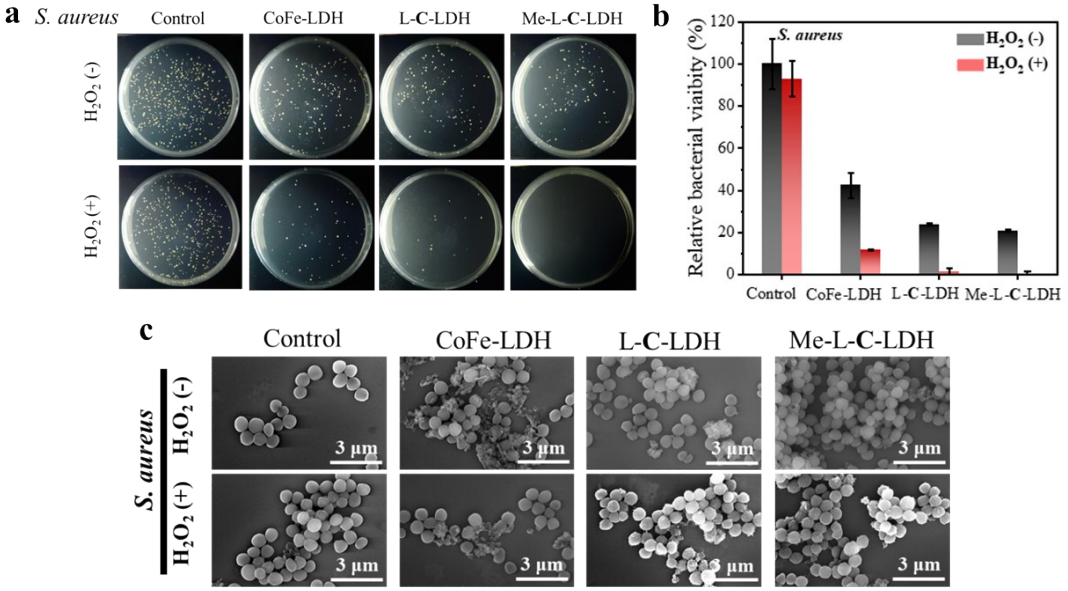

Figure S52. (a) Photographs of bacterial colonies formed by *S. aureus* after exposure to control, different nanozymes (CoFe-LDH, L-**C**-LDH and Me-L-**C**-LDH) and different nanozymes with the addition of H_2O_2. The working concentrations for nanozyme, H_2O_2, and acetate buffer were 200 μg mL^{-1}, 0.5 mM and 0.1 M, respectively. (b) Corresponding bacterial viability measurement of *S. aureus* upon different treatments. (c) SEM images of *S. aureus* upon different treatments.

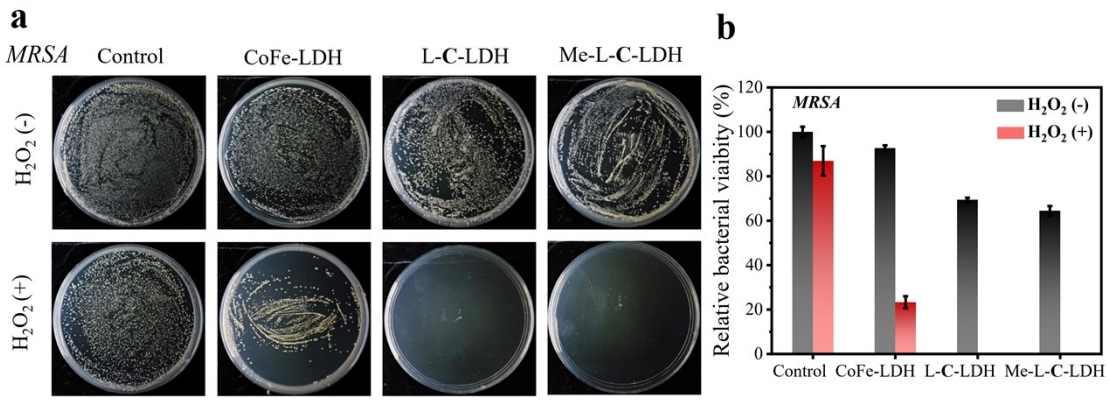

Figure S53. (a) Photograph of bacterial colonies formed by *MRSA* after exposure to control, different nanozymes (CoFe-LDH, L-**C**-LDH and Me-L-**C**-LDH), nanozymes+H_2O_2. The working concentrations for nanozymes, H_2O_2, and sodium acetate buffer are 250 μg mL^{-1}, 0.5 mM and 0.1 M, respectively. (b) Corresponding bacterial viability measurement of *MRSA* upon different treatments.

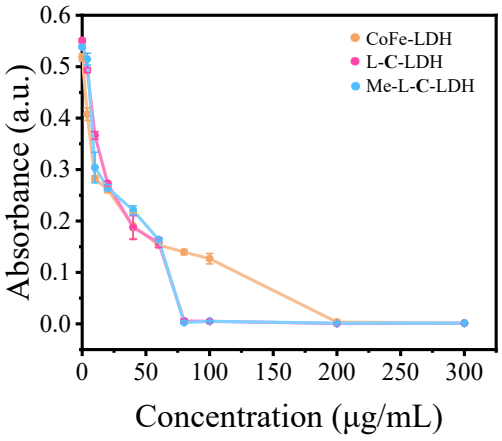

Figure S54. The OD_{600} of *E. coli* liquid medium treated with different concentrations of CoFe-LDH nanozyme, L-**C**-LDH nanozyme and Me-L-**C**-LDH nanozyme in the presence of H_2O_2 (1 mM).

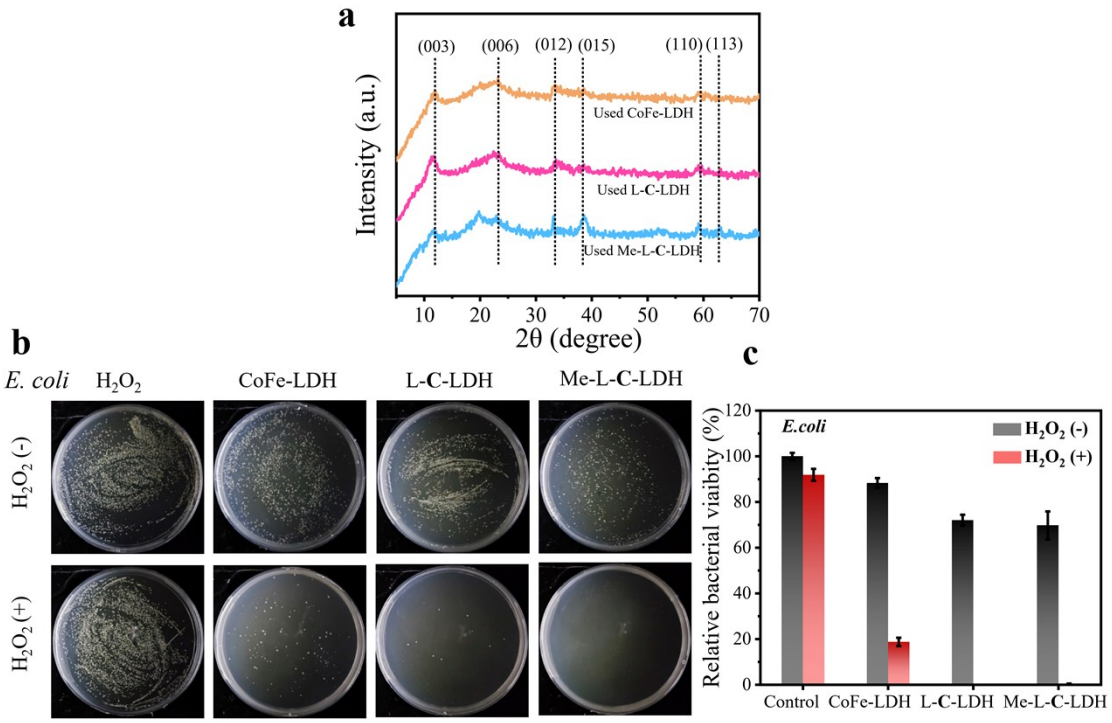

Figure S55. (a) PXRD pattern of used LDH nanozymes. (b) Photographs of bacterial colonies formed by *E. coli* after exposure to control, different used nanozymes with the addition of H_2O_2. (c) Corresponding bacterial viability measurement of *E. coli* upon different treatments.

Table S1. Elemental analysis (ICP) of different LDH nanozymes.

Materials	Co (%)	Fe (%)	S (%)
CoFe-LDH	42.37	15.01	-
L-**C**-LDH	34.98	14.48	3.41
Me-L-**C**-LDH	33.82	14.48	3.07

Table S2. Indexing of XRD patterns for CoFe-LDH nanozyme and L-AA-LDH nanozymes.

L-AA-LDH	d_{003}/nm	d_{006}/nm	d_{012}/nm	d_{110}/nm	lattice parameter a/nm	lattice parameter c/nm
CoFe-LDH	**0.767**	**0.387**	**0.262**	**0.156**	**0.312**	**2.301**
L-**A**-LDH	0.795	0.396	0.265	0.157	0.314	2.385
L-**R**-LDH	0.789	0.394	0.269	0.156	0.312	2.367
L-**N**-LDH	0.794	0.395	0.265	0.156	0.312	2.382
L-**D**-LDH	0.785	0.393	0.269	0.156	0.312	2.355
L-**C**-LDH	0.799	0.399	0.266	0.156	0.312	2.397
L-**Q**-LDH	0.802	0.393	0.266	0.157	0.314	2.406
L-**E**-LDH	0.790	0.394	0.270	0.156	0.312	2.370
L-**G**-LDH	0.802	0.397	0.267	0.156	0.312	2.406
L-**H**-LDH	0.772	0.461	0.271	0.156	0.312	2.316
L-**I**-LDH	0.789	0.390	0.264	0.156	0.312	2.367
L-**L**-LDH	0.787	0.460	0.270	0.156	0.312	2.361
L-**K**-LDH	0.787	0.397	0.266	0.156	0.312	2.361
L-**M**-LDH	0.789	0.394	0.266	0.156	0.312	2.367
L-**F**-LDH	0.776	0.458	0.270	0.156	0.312	2.328
L-**P**-LDH	0.778	0.458	0.270	0.156	0.312	2.334
L-**S**-LDH	0.787	0.389	0.270	0.156	0.312	2.361
L-**T**-LDH	0.785	0.393	0.265	0.156	0.312	2.355
L-**W**-LDH	0.787	0.461	0.271	0.156	0.312	2.361
L-**Y**-LDH	0.785	0.455	0.271	0.156	0.312	2.355
L-**V**-LDH	0.785	0.459	0.270	0.156	0.312	2.355

Table S3. Indexing of XRD patterns for **C**-LDH nanozymes.

C-LDH	d_{003}/nm	d_{006}/nm	d_{012}/nm	d_{110}/nm	lattice parameter a/nm	lattice parameter c/nm
L-**C**-LDH	0.799	0.399	0.266	0.156	0.312	2.397
L-**C**-LDH (HCl)	0.779	0.393	0.265	0.156	0.312	2.337
D-**C**-LDH	0.784	0.392	0.266	0.156	0.312	2.352
Acet-L-**C**-LDH	0.782	0.388	0.267	0.155	0.310	2.346
Me-L-**C**-LDH	0.804	0.389	0.265	0.156	0.312	2.412
Et-L-**C**-LDH	0.791	0.390	0.263	0.156	0.312	2.373
C-**C**-LDH	0.794	0.390	0.265	0.156	0.312	2.382
L-**M**-LDH	0.793	0.394	0.267	0.156	0.312	2.379

Table S4. Comparison of the Michaelis-Menten constant (K_m) and maximum reaction rate (V_{max}).

Samples	K_m (mM)		V_{max} ($\times 10^{-8}$ M s^{-1})		Ref.
	H_2O_2	TMB	H_2O_2	TMB	
HRP (37℃)	3.70	0.434	8.71	10.00	[13]
Fe_3O_4	1.54	0.098	9.78	3.44	[13]
Co_3O_4 NPs	140.07	0.037	12.1	6.27	[14]
Co_3O_4@Co-Fe oxide DSNCs	0.24	0.48	5.18	5.32	[15]
$Pc(OH)_8$-CoFe-LDH	1.55	0.361	4.760	12.456	[16]
MXene@NiFe-LDH	0.078	0.187	2.076	1.707	[17]
CoAl-ELDH	22.13	0.372	0.598	0.101	[18]
CoFe-LDH/CeO_2	10.82	0.419	-	-	[19]
CoFe-LDH	-	0.09	-	2.53	[20]
CoFeMn-LDH	-	1.11	-	17.35	[21]
DNA/CuAl-LDH	10.24	1.775	2.30	4.09	[22]
Pt/NiCo-LDH	14.94	0.16	76.10	132.80	[23]
FeNiCo-LDH	0.085	4.17	11.63	60.28	[24]
NiCo-LDH (6:4)	6.412	-	2.802	-	[25]
Ni-MOF@NiV-LDHs	0.007	0.120	2.54	4.33	[4]
100CuNiAl LDH	1.26	0.15	1.28	0.77	[26]
CDs/LDHzyme	4.209	237.2	20.02	6.166	[27]
GTP/FeCo-LDH@WO_3	0.4	0.17	15.00	22.00	[28]
Fe/Ni-LDH	4.905	-	5.015	-	[29]
Ru_1/LDH SAE	0.104	0.121	142.00	189.00	[30]
$Ni_{0.67}Mn_{0.33}$ LDH	0.062	0.32	44.6	74.88	[31]
Fe/NC-SAs	38.62	0.091	48.65	33.35	[32]
Au/Co_3O_4-CeO_x (45°C)	0.2724	0.1219	0.3898	0.8577	[33]
$NiCo_2O_4$ MS (37°C)	9.406	0.142	25.840	2.223	[34]
MOF (Co/2Fe)	4.22	0.250	4.91	3.78	[35]
CoFe-LDH (25°C)	0.293	1.601	31.65	27.06	this work
L-**C**-LDH (25°C)	0.624	1.076	63.03	126.09	this work
Me-L-**C**-LDH (25°C)	0.314	1.457	81.26	129.24	this work
CoFe-LDH (37°C)	0.320	1.268	72.01	113.8	this work
L-**C**-LDH (37°C)	0.436	1.613	140.9	206.1	this work
Me-L-**C**-LDH (37°C)	0.959	3.539	140.7	277.8	this work

Table S5. EXAFS fitting parameters at the Co K-edge for CoFe-LDH nanozyme, L-**C**-LDH nanozyme and Me-L-**C**-LDH nanozyme.

Sample	Shell	CN	R (Å)	σ^2 (10^{-3}Å^2)	$\triangle E_0$ (eV)	R factor
CoFe-LDH	Co-O	8.5±0.7	2.07±0.01	9.5	-3.7±0.4	0.0069
	Co-Co/Fe	11.2±1.4	3.14±0.01	11.3	-1.9±0.4	
L-**C**-LDH	Co-O	8.4±1.0	2.07±0.01	12.2	-2.9±0.5	0.0128
	Co-Co/Fe	6.7±1.3	3.14±0.01	9.0	-0.4±0.7	
Me-L-**C**-LDH	Co-O	6.7±0.2	2.07±0.01	8.4	-2.0±0.2	0.0046
	Co-Co/Fe	9.7±0.3	3.14±0.01	11.7	-1.2±0.3	

Table S6. EXAFS fitting parameters at the Fe K-edge for CoFe-LDH nanozyme, L-**C**-LDH nanozyme and Me-L-**C**-LDH nanozyme.

Sample	Shell	CN	R (Å)	σ^2 (10^{-3}Å^2)	$\triangle E_0$ (eV)	R factor
CoFe-LDH	Fe-O	7.4±0.8	2.02±0.01	6.5	-0.9±0.6	0.0055
	Fe-Fe	8.8±2.2	3.14±0.01	10.2	-0.1±0.8	
L-**C**-LDH	Fe-O	5.9±0.7	2.02±0.01	7.4	-2.7±0.6	0.0074
	Fe-Fe	3.8±1.2	3.14±0.01	8.3	-1.2±1.0	
Me-L-**C**-LDH	Fe-O	5.8±0.4	1.98±0.01	5.6	-5.9±0.3	0.0021
	Fe-Fe	5.1±0.8	3.15±0.01	7.2	-0.6±0.5	

CN, coordination number; R, bond distance; σ^2, Debye-Waller factor to account for both thermal and structural disorders; ΔE_0, inner potential correction; R factor indicates the goodness of the fit.

Table S7. Comparison of nanozymes with POD-like activity for the colorimetric detection of H_2O_2.

Nanozyme	Linear range (μM)	LOD (μM)	Ref.
GTP/FeCo-LDH@WO_3	0.1-100	11	[28]
Au/Co_3O_4-CeO_x	10-1000	5.29	[33]
Fe-MoS_2	1.0-200	0.20	[36]
Fe-CQDs	0.5-40	0.147	[37]
L-**C**-LDH	5-100	0.78	this work
Me-L-**C**-LDH	5-100	0.42	this work

Table S8. Comparison of different nanozymes for the detection of AA.

Materials	Methods	Linear range (μM)	LOD (μM)	Ref.
Ni/C	electrochemical	20-2400	5	[38]
CoOOH-CDs-p-PD	fluorimetry	0.5-10	0.09	[39]
SiQDs-MnO_2 NS	fluorimetry	1-80	0.48	[40]
MnFe-LDH	fluorimetry	0.5-2.5	0.16	[41]
d-CoFe-LDHs	colorimetry	20-625	3.6	[42]
CoOOH	colorimetry	0.5-50	0.14	[43]
Cu-BDC-NH_2 NPs	colorimetry	0.5-60	0.15	[44]
CNFs/$MnCo_2O_{4.5}$	colorimetry	0-40	0.05	[45]
L-**C**-LDH	colorimetry	0.05-1	0.024	this work
Me-L-**C**-LDH	colorimetry	0.05-1	0.027	this work

Table S9. The content of amino acid intercalated in L-**C**-LDH nanozyme and Me-L-**C**-LDH nanozyme.

Materials	Amino acid (wt%)
L-**C**-LDH	3.65±0.26
Me-L-**C**-LDH	3.16±0.10

References

[1] X. Zhang, L. Yan, J. Li, H. Yu, Adsorption of heavy metals by L-cysteine intercalated layered double hydroxide: Kinetic, isothermal and mechanistic studies, J. Colloid Interf. Sci. 562 (2020) 149-158.

[2] P. Wang, L. Yin, X. Wang, G. Zhao, S. Yu, G. Song, J. Xie, A. Alsaedi, T. Hayat, X. Wang, L-cysteine intercalated layered double hydroxide for highly efficient capture of U(VI) from aqueous solutions, J. Environ. Manag. 217 (2018) 468-477.

[3] M. Chen, X. Zhou, C. Xiong, T. Yuan, W. Wang, Y. Zhao, Z. Xue, W. Guo, Q. Wang, H. Wang, Y. Li, H. Zhou, Y. Wu, Facet engineering of nanoceria for enzyme-mimetic catalysis, ACS Appl. Mater. Interfaces 14 (2022) 21989-21995.

[4] Y. He, M. Feng, X. Zhang, Y. Huang, Metal-organic framework (MOF)-derived flower-like Ni-MOF@NiV-layered double hydroxides as peroxidase mimetics for colorimetric detection of hydroquinone, Anal. Chim. Acta 1283 (2023) 341959.

[5] P. Hohenberg, W. Kohn, Inhomogeneous electron gas, Phys. Rev. 136 (1964) B864-B871.

[6] W. Kohn, L.J. Sham, Self-consistent equations including exchange and correlation effects, Phys. Rev. 140 (1965) A1133-A1138.

[7] G. Kresse, J. Furthmüller, Efficient iterative schemes for ab initio total-energy calculations using a plane-wave basis set. Phys. Rev. B 54 (1996) 11169

[8] P.E. Blöchl, Projector augmented-wave method, Phys. Rev. B 50 (1994) 17953-17979.

[9] J.P. Perdew, K. Burke, M. Ernzerhof, Generalized gradient approximation made simple. Phys. Rev. Lett. 77 (1996) 3865.

[10] S. Grimme, J. Antony, S. Ehrlich, H. Krieg, A consistent and accurate ab initio parametrization of density

functional dispersion correction (DFT-D) for the 94 elements H-Pu, J. Chem. Phys. 132 (2010) 154104.

[11] Y. Ma, K. Jiang, H. Chen, Q. Shi, H. Liu, X. Zhong, H. Qian, X. Chen, L. Cheng, X. Wang, Liquid exfoliation of V_8C_7 nanodots as peroxidase-like nanozymes for photothermal-catalytic synergistic antibacterial treatment, Acta Biomater. 149 (2022) 359-372.

[12] H. Wang, F. Lu, C. Ma, Y. Ma, M. Zhang, B. Wang, Y. Zhang, Y. Liu, H. Huang, Z. Kang, Carbon dots with positive surface charge from tartaric acid and m-aminophenol for selective killing of Gram-positive bacteria, J. Mater. Chem. B 9 (2021) 125-130.

[13] L. Gao, J. Zhuang, L. Nie, J. Zhang, Y. Zhang, N. Gu, T. Wang, J. Feng, D. Yang, S. Perrett, X. Yan, Intrinsic peroxidase-like activity of ferromagnetic nanoparticles, Nat. Nanotechnol. 2 (2007) 577-583.

[14] J. Mu, Y. Wang, M. Zhao, L. Zhang, Intrinsic peroxidase-like activity and catalase-like activity of Co_3O_4 nanoparticles, Chem. Commun. 48 (2012) 2540-2542.

[15] Q. Chen, X. Zhang, S. Li, J. Tan, C. Xu, Y. Huang, MOF-derived Co_3O_4@Co-Fe oxide double-shelled nanocages as multi-functional specific peroxidase-like nanozyme catalysts for chemo/biosensing and dye degradation, Chem. Eng. J. 395 (2020) 125130.

[16] P. Hao, Y. Liu, S. Dong, G. Fan, G. Li, M. Xie, Q. Liu, Enhanced peroxidase-like activity of 2(3), 9(10), 16(17), 23(24)-octamethoxyphthalocyanine modified CoFe LDH for a sensor array for reducing substances with catechol structure, Anal. Bioanal. Chem. 415 (2022) 289-301.

[17] H. Li, Y. Wen, X. Zhu, J. Wang, L. Zhang, B. Sun, Novel Heterostructure of a MXene@NiFe-LDH nanohybrid with superior peroxidase-like activity for sensitive colorimetric detection of glutathione, ACS Sustain. Chem. Eng. J. 8 (2019) 520-526.

[18] L. Chen, B. Sun, X. Wang, F. Qiao, S. Ai, 2D ultrathin nanosheets of Co-Al layered double hydroxides prepared in L-asparagine solution: enhanced peroxidase-like activity and colorimetric detection of glucose, J. Mater. Chem. B 1 (2013) 2268-2274.

[19] W. Yang, J. Li, J. Yang, Y. Liu, Z. Xu, X. Sun, F. Wang, D.H.L. Ng, Biomass-derived hierarchically porous CoFe-LDH/CeO_2 hybrid with peroxidase-like activity for colorimetric sensing of H_2O_2 and glucose, J. Alloy. Compd. 815 (2020) 152276.

[20] D. Yin, S. Zheng, X. Xu, F. Wang, L. Wang, Fluorescence/colorimetry/smartphone triple-mode sensing platform based on carbon dots and Co, Fe-layered double hydroxides for citrate determination, Sensor. Actuat. B: Chem. 397 (2023) 134706.

[21] H. Shang, X. Zhang, M. Ding, A. Zhang, C. Wang, Dual-Mode paper biosensing platform based on oxidase-like CoFeMn nanozymes for point-of-care detection of glutathione, ACS Appl. Nano Mater. 6(10) (2023) 8907-8915.

[22] L. Chen, K. Sun, P. Li, X. Fan, J. Sun, S. Ai, DNA-enhanced peroxidase-like activity of layered double hydroxide nanosheets and applications in H_2O_2 and glucose sensing, Nanoscale 5 (2013) 10982-10988.

[23] X. Cao, H. Yang, Q. Wei, Y. Yang, M. Liu, Q. Liu, X. Zhang, Fast colorimetric sensing of H_2O_2 and glutathione based on Pt deposited on NiCo layered double hydroxide with double peroxidase-/oxidase-like activity, Inorga. Chem. Commun. 123 (2021) 108331.

[24] Y. Qin, S. Li, L. Liang, S. Zhao, F. Ye, Rational synthesis of FeNiCo-LDH nanozyme for colorimetric detection of deferoxamine mesylate, Spectrochim. Acta A 303 (2023) 123156.

[25] L. Su, S. Qin, X. Yu, Y. Chen, L. Wang, W. Dong, Z. Xie, H. Zhang, NiCo LDH nanozymes with selective antibacterial activity against Gram-negative bacteria for wound healing, J. Mater. Chem. B 11 (2023) 7675-7683.

[26] L. Wu, X. Zhou, G. Wan, Y. Tang, S. Shi, X. Xu, G. Wang, Novel hierarchical CuNiAl LDH nanotubes with excellent peroxidase-like activity for wide-range detection of glucose, Dalton Trans. 50 (2021) 95-102.

[27] R. Wang, Y. Yu, R. Zhang, X. Ren, W. Guo, Vacancy-rich structure inducing efficient persulfate activation for tetracycline degradation over Ni-Fe layered double hydroxide nanosheets, Sep. Purif. Techno. 289 (2022) 120663.

[28] S. Dadakhani, G. Dehghan, A. Khataee, A robust and facile label-free method for highly sensitive colorimetric detection of ascorbic acid in fresh fruits based on peroxidase-like activity of modified FeCo-LDH@WO_3 nanocomposite, Spectrochim. Acta A 302 (2023) 123016.

[29] Q. Pan, F. Lin, R. Liu, Y. Li, X. Zhang, R. Luo, L. Cai, Y. Liu, W. Deng, L. He, Fe/Ni layered double hydroxide biocatalysts inhibit tumor growth through ROS and ferroptosis signaling pathway, Chem. Eng. J. 466 (2023) 142962.

[30] B. Wang, Y. Fang, X. Han, R. Jiang, L. Zhao, X. Yang, J. Jin, A. Han, J. Liu, Atomization-induced high intrinsic activity of a biocompatible MgAl-LDH supported ru single-atom nanozyme for efficient radicals scavenging, Angew. Chem. Int. Ed. 62 (2023) e202307133

[31] Y. Sun, H. Xu, L. Wang, C. Yu, J. Zhou, Q. Chen, G. Sun, W. Huang, Ultrathin NiMn layered double hydroxide nanosheets with a superior peroxidase mimicking performance to natural HRP for disposable paper-based bioassays, J. Mater. Chem. B 9 (2021) 983-991.

[32] X. Xie, Y. Wang, X. Zhou, J. Chen, M. Wang, X. Su, Fe-N-C single-atom nanozymes with peroxidase-like activity for the detection of alkaline phosphatase, The Analyst 146 (2021) 896-903.

[33] H. Liu, Y. Ding, B. Yang, Z. Liu, Q. Liu, X. Zhang, Colorimetric and ultrasensitive detection of H_2O_2 based on Au/Co_3O_4-CeO_x nanocomposites with enhanced peroxidase-like performance, Sensor. Actuat. B: Chem. 271 (2018) 336-345.

[34] L. Su, W. Dong, C. Wu, Y. Gong, Y. Zhang, L. Li, G. Mao, S. Feng, The peroxidase and oxidase-like activity of $NiCo_2O_4$ mesoporous spheres: Mechanistic understanding and colorimetric biosensing, Anal. Chim. Acta 951 (2017) 124-132.

[35] H. Yang, R. Yang, P. Zhang, Y. Qin, T. Chen, F. Ye, A bimetallic (Co/2Fe) metal-organic framework with oxidase and peroxidase mimicking activity for colorimetric detection of hydrogen peroxide, Microchim. Acta 184 (2017) 4629-4635.

[36] L. Feng, L. Zhang, S. Chu, S. Zhang, X. Chen, Z. Du, Y. Gong, H. Wang, Controllable doping of Fe atoms into MoS_2 nanosheets towards peroxidase-like nanozyme with enhanced catalysis for colorimetric analysis of glucose, Appl. Surf. Sci. 583 (2022) 152496.

[37] X. Huang, M. Jiang, H. Zeng, J. Wu, J. Wu, X. Liu, L. Zhou, Y. Yuan, Autogenous iron-based peroxidase-like nanozyme from paper mill sludge for ascorbic acid detection, Mater. Today Commun. 36 (2023) 106775.

[38] W. He, Y. Ding, W. Zhang, L. Ji, X. Zhang, F. Yang, A highly sensitive sensor for simultaneous determination of ascorbic acid, dopamine and uric acid based on ultra-small Ni nanoparticles, J. Electroanal. Chem. 775 (2016) 205-211.

[39] N. Li, Y.Q. Zhong, S.G. Liu, Y.Q. He, Y.Z. Fan, J.H. Hu, X. Mai, Smartphone assisted colorimetric and fluorescent triple-channel signal sensor for ascorbic acid assay based on oxidase-like CoOOH nanoflakes, Spectrochim. Acta A 238 (2020) 118412.

[40] F. Ma, J. Luo, X. Li, S. Liu, M. Yang, X. Chen, A “switch-on” fluorescence assay based on silicon quantum dots for determination of ascorbic acid, Spectrochim. Acta A 249 (2021) 119343.

[41] C. Peng, H. Xing, Y. Xue, J. Wang, J. Li, E. Wang, Ratiometric sensing of alkaline phosphatase based on the catalytical activity from Mn-Fe layered double hydroxide nanosheets, Nanoscale 12 (2020) 2022-2027.

[42] Y. Ning, Y. Sun, X. Yang, Y. Li, A. Han, B. Wang, J. Liu, Defect-rich CoFe-layered double hydroxides as superior peroxidase-like nanozymes for the detection of ascorbic acid, ACS Appl. Mater. Interf. 15 (2023) 26263-26272.

[43] D. Ji, Y. Du, H. Meng, L. Zhang, Z. Huang, Y. Hu, J. Li, F. Yu, Z. Li, A novel colorimetric strategy for sensitive and rapid sensing of ascorbic acid using cobalt oxyhydroxide nanoflakes and 3,3′,5,5′-tetramethylbenzidine, Sensor. Actuat. B: Chem. 256 (2018) 512-519.

[44] Z. Yao, Z. Li, H. Liu, Y. Liu, Y. Sun, Z. Li, A novel colorimetric assay based on the peroxidase-like properties of amino functionalized copper metal-organic framework nanoparticles for ascorbic acid sensing, Anal. Methods 11 (2019) 1697-1706.

[45] M. Gao, X. Lu, G. Nie, M. Chi, C. Wang, Hierarchical CNFs/$MnCo_2O_{4.5}$ nanofibers as a highly active oxidase mimetic and its application in biosensing, Nanotechnology. 28 (2017) 485708.